AIAA JOURNAL
Vol. 45, No. 6, June 2007

Adaptation of Aeroelastic Reduced-Order Models and Application to an F-16 Configuration

Thuan Lieu* and Charbel Farhat†
Stanford University, Stanford, California 94305-3035

DOI: 10.2514/1.24512

The proper orthogonal decomposition method has been shown to produce accurate reduced-order models for the aeroelastic analysis of complete aircraft configurations at fixed flight conditions. However, changes in the Mach number or angle of attack often necessitate the reconstruction of the reduced-order model to maintain accuracy, which destroys the sought-after computational efficiency. Straightforward approaches for reduced-order model adaptation—such as the global proper orthogonal decomposition method and the direct interpolation of the proper orthogonal decomposition basis vectors—that have been attempted in the past have been shown to lead to inaccurate proper orthogonal decomposition bases in the transonic flight regime. Alternatively, a new reduced-order model adaptation scheme is described in this paper and evaluated for changes in the freestream Mach number and angle of attack. This scheme interpolates the subspace angles between two proper orthogonal decomposition subspaces, then generates a new proper orthogonal decomposition basis through an orthogonal transformation based on the interpolated subspace angles. The resulting computational methodology is applied to a complete F-16 configuration in various airstreams. The predicted aeroelastic frequencies and damping coefficients are compared with counterparts obtained from full-order nonlinear aeroelastic simulations and flight test data. Good correlations are observed, including in the transonic regime. The obtained computational results reveal a significant potential of the adapted reduced-order model computational technology for accurate, near-real-time, aeroelastic predictions.

Nomenclature

$\mathbf{A}$ ($\bar{\mathbf{A}}$)	=	matrix of (adimensional) cell volumes obtained from a finite volume discretization of the fluid subsystem
$\bar{\mathbf{B}}_r$	=	adimensional reduced-order aeroelastic coupling matrix
$\mathbf{C}$ ($\bar{\mathbf{C}}$)	=	gradient of the (adimensional) cell volumes with respect to the (adimensional) fluid mesh motion
$\mathbb{C}^n$	=	complex plane of dimension n
$\mathbf{D}_o$	=	finite element damping matrix obtained by linearizing the internal force vector with respect to the structural velocities
$\mathbf{E}$ ($\bar{\mathbf{E}}$)	=	gradient of the (adimensional) flux function with respect to the (adimensional) fluid mesh velocity
$\mathbf{e}_k$	=	kth interpolated principal subspace vector
$\mathbf{F}$ ($\bar{\mathbf{F}}$)	=	nonlinear (adimensional) numerical fluid flux function
$\mathbf{f}^{\text{ext}}$	=	vector of external forces applied to the structural subsystem
$\mathbf{f}^{\text{int}}$	=	vector of internal forces of the structural subsystem
$\mathbf{G}$ ($\bar{\mathbf{G}}$)	=	gradient of the (adimensional) flux function with respect to the (adimensional) fluid mesh displacement
$\mathbf{H}$ ($\bar{\mathbf{H}}$)	=	first-order term of the Taylor expansion of the (adimensional) numerical fluid flux function
$\bar{\mathbf{H}}_r$	=	adimensional reduced-order fluid subsystem matrix
$\mathbf{I}$	=	identity matrix
i	=	imaginary number satisfying $i^2 = -1$
$\bar{\mathbf{K}}$	=	adimensional fictitious stiffness matrix of the pseudostructural fluid mesh
$\tilde{\mathbf{K}}$	=	adimensional fictitious stiffness matrix of the mesh motion subsystem
$\tilde{\mathbf{K}}_c$	=	transfer matrix relating the nodal motions at the fluid/structure interface
$\mathbf{K}_s$	=	adjusted finite element stiffness matrix for the linearized structural equations
$\mathbf{K}_o$	=	finite element stiffness matrix obtained by linearizing the internal force vector with respect to the structural displacements
k	=	reduced frequency defined by $k = (L_r/v_r)\omega$
L_r	=	reference length
$\mathbf{M}$	=	finite element mass matrix of the structural subsystem
$\mathcal{M}, \mathcal{N}$	=	subspaces of $\mathbb{C}^n$
M_∞	=	freestream Mach number
$\mathbf{P}$	=	linearization of the external load with respect to the adimensional fluid state vector
$\mathbf{P}_m$	=	generalized external force matrix
$\mathbf{R}$	=	correlation matrix
$\mathbf{S}$	=	real-valued snapshot matrix
$,t$	=	partial derivative with respect to time t
$\mathbf{U}$, $\mathbf{V}$	=	matrix of principal subspace vectors
$\mathbf{u}$	=	vector of structural displacements or POD principal basis vector
$\bar{\mathbf{u}}$	=	adimensional vector of structural displacements
$\mathbf{u}_m$	=	generalized (modal) displacement coordinates of the structure
$\mathbf{v}$	=	POD principal basis vector
v_r	=	reference velocity
$\mathbf{W}$	=	adimensional complex-valued snapshot matrix
$\mathbf{w}$ ($\bar{\mathbf{w}}$)	=	(adimensional) conservative state vector of the fluid subsystem
$\mathbf{x}$ ($\bar{\mathbf{x}}$)	=	vector of (adimensional) fluid nodal displacements
$\dot{\mathbf{x}}$ ($\dot{\bar{\mathbf{x}}}$)	=	vector of (adimensional) fluid mesh nodal velocities
$\mathbf{Y}$	=	matrix of left singular value decomposition vectors
$\bar{\mathbf{y}}_r$	=	adimensional reduced-order vector of structural displacements and velocities
$\mathbf{Z}$	=	matrix of right singular value decomposition vectors
α	=	angle of attack

Received 7 April 2006; revision received 14 February 2007; accepted for publication 16 February 2007.

*Post-Doctoral Scholar, Institute for Computational and Mathematical Engineering, Building 500, 488 Escondido Mall. Member AIAA.

†Professor, Department of Mechanical Engineering, Institute for Computational and Mathematical Engineering, and Department of Aeronautics and Astronautics (by courtesy), Building 500, 488 Escondido Mall. Fellow AIAA.

$\Delta(\,)$ = indicates a perturbed quantity from a linearization point
θ_k ($\tilde{\theta}_k$) = (interpolated) principal subspace angles
Λ = matrix of eigenvalues of the correlation matrix
$\mathbf{\Sigma}$ = matrix of singular values
$,\tau$ = partial derivative with respect to adimensional time τ
$\mathbf{\Phi}$ = matrix of POD basis vectors
$\mathbf{\Phi}_r$ = truncated POD basis vectors
$\mathbf{\Psi}$ = eigenvectors of the alternative correlation matrix eigenvalue problem
$\mathbf{\Omega}$ = diagonal matrix of the natural pulsations of the structural subsystem
ω = angular frequency
$\dot{(\,)}$ = partial derivative with respect to time

I. Introduction

IN THE transonic flight regime, state-of-the-art computational fluid dynamics (CFD)-based nonlinear simulation technologies [1–4] have become a superior choice over linear computational methods [5,6] for aeroelastic analysis. They have also become a viable alternative to scaled wind-tunnel testing for flutter prediction. For example, the AERO code was reported to accurately predict the aeroelastic parameters of a complete F-16 configuration at five different Mach numbers in the transonic regime, in less than one day using a 128-processor machine, and in less than three days using an eight-processor computing platform [3,4]. Such performance meets the nonlinear aeroelastic challenge recently formulated in [7]. However, it is insufficient for enabling routine aeroelastic analyses in design and test operations, due to the still lengthy simulation time.

The major computational cost incurred by CFD-based nonlinear aeroelastic simulations is attributable to the need for high-fidelity fluid models to resolve the complex flow patterns present in the transonic regime. Because of this computational cost, the potential of CFD-based nonlinear aeroelastic codes is currently limited to the analysis of a few, carefully chosen configurations rather than routine analysis. In some instances such as those discussed later in this paper, it is possible, however, to address this limitation with the use of reduced-order models (ROMs). For example, it was recently shown [8–18] that ROMs constructed by a variety of methods can produce numerical results that compare well with those generated by full-order nonlinear models. In particular, the popular proper orthogonal decomposition (POD) method [19,20] has been successfully applied to simple airfoils [10–12,14], panels [21], wings [13,15,16], turbine blades [17,18], and most recently to complete aircraft configurations [22,23]. However, one aspect of ROMs that should not be ignored is that, often, their construction requires a significant amount of computational resources. For example, both the POD and Volterra series [24] approaches can be CPU intensive as they require accumulating system responses from numerical simulations based on the full-order computational model. Furthermore, a ROM constructed by POD or any other similar technique is usually not robust with respect to changes in a model parameter [14,25]. In principle, it should be reconstructed whenever a model parameter is updated. To avoid this overhead cost, ROM adaptation algorithms are needed. Some progress in this area has been recently reported for the case of structural parameters [15]; however, with few exceptions [14,16,23,26–28] little has been reported for changes in the freestream Mach number and angle of attack. Hence, the objectives of this paper are twofold: 1) to overview the results of a POD-based ROM methodology for the CFD-based aeroelastic analysis of a complete fighter configuration, including in the transonic regime, and 2) to present and analyze an algorithm for rapidly adapting aeroelastic ROMs to changes in the freestream Mach number and angle of attack. To this effect, the remainder of this paper is organized as follows.

In Sec. II, the computational framework adopted for constructing a POD-based ROM is presented. In Sec. III, a novel algorithm for adapting two given ROMs to changes in the freestream Mach number and/or angle of attack is described. This algorithm is contrasted with two other adaptation methods, namely, the global POD (GPOD) and direct basis interpolation methods. In Sec. IV, the proposed ROM computational technology is applied to the aeroelastic analysis of a complete F-16 configuration at low angles of attack. The aeroelastic parameters obtained using the ROMs are compared with those obtained using full-order nonlinear simulations and flight test data. Finally, conclusions pertaining to the performance characteristics, merits, limitations, and potential of the described computational methodologies are formulated in Sec. V.

II. Nonlinear and Linearized Computational Frameworks

To construct a POD subspace, an ensemble of sample data representative of some physical system—in this case, a flexible aircraft—is required. These sample data are generated here by numerical simulation in the frequency domain of the linearized flows associated with a set of excitations of the displacement field of the structural model of the aircraft. To this effect, the transient aeroelastic problem is first formulated as a coupled, nonlinear, fluid/structure interaction problem. However, to facilitate the application of the POD method, this nonlinear formulation is then linearized around a steady-state solution determined by the freestream Mach number and angle of attack (assuming a fixed yaw angle). Although the main objective of aeroelastic reduced-order modeling is to reduce the size of the coupled aeroelastic system, model reduction is performed here separately for the individual fluid and structural subsystems. This decoupled approach has several advantages. First, it allows using the most suitable ROM approach for each separate subsystem. For example, a modal-based ROM is as effective for a structural subsystem as a POD-based one and simpler to construct. Furthermore, this approach allows formulating the fluid subsystem in adimensionalized form so that the resulting POD basis is independent of the freestream pressure and density, thus making the resulting fluid ROM independent of altitude. This robustness with respect to changes in the freestream density and/or pressure would be more difficult to achieve if reduced-order modeling were to be applied to the coupled aeroelastic system in a monolithic fashion, because the state of the coupled system depends on these freestream parameters.

For simplicity but without any lack of generality, the flow is assumed to be inviscid throughout the remainder of this paper. The three-field arbitrary Lagrangian–Eulerian (ALE) formulation of fluid/structure interaction problems popularized by Farhat et al. [29] is adopted for all full-order nonlinear aeroelastic simulations. An extension of the linearization of this formulation introduced by Lesoinne et al. [30] is chosen as the computational framework for POD calculations. The main steps of the POD algorithm closely follow the procedure set forth in previous works [9,10,15,31], but are adapted to fit within the chosen computational framework.

A. Governing Equations

A nonlinear aeroelastic system can be represented by the three-field ALE formulation [29] of fluid/structure interaction problems. After semidiscretization by a combination of finite element (FE) and finite volume methods, this formulation gives rise to three coupled ordinary differential equations of the form:

$$(\mathbf{A}(\mathbf{x})\mathbf{w})_{,t} + \mathbf{F}(\mathbf{w}, \mathbf{x}, \dot{\mathbf{x}}) = 0 \tag{1}$$

$$\mathbf{M}\,\ddot{\mathbf{u}} + \mathbf{f}^{\text{int}}(\mathbf{u}, \dot{\mathbf{u}}) = \mathbf{f}^{\text{ext}}(\mathbf{u}, \mathbf{w}) \tag{2}$$

$$\tilde{\mathbf{K}}\mathbf{x} = \tilde{\mathbf{K}}_c\mathbf{u} \tag{3}$$

Here, Eq. (1) represents a finite volume discretization of the ALE conservation form of the fluid equations. Equation (2) is a FE discretization of the structural equations of dynamic equilibrium. The various Dirichlet and Neumann boundary conditions associated with the fluid and structural subproblems are embedded in the above system and, for simplicity, are not explicitly stated. In many aeroelastic applications, the boundary of the fluid domain is required

to deform according to the motion of the wet surface of the structure. This is represented here by Eq. (3) which models the fluid mesh as a pseudostructure with a quasistatic behavior [32]. The transfer matrix $\tilde{\mathbf{K}}_c$ describes the effect of structural motions on the fluid mesh at the fluid-structure interface [33]. For the purpose of constructing a ROM, the above formulation of an aeroelastic problem is simplified as follows.

First, both the fluid and structural equations are linearized around an equilibrium point designated by the subscript o and satisfying $\dot{\mathbf{w}}_o = \dot{\mathbf{x}}_o = 0$, following the approach described first in [30,34]. Equation (1) is perturbed about an equilibrium configuration $(\mathbf{w}_o, \dot{\mathbf{w}}_o, \mathbf{x}, \dot{\mathbf{x}}_o)$ so that

$$\mathbf{w}(M_\infty, \alpha) = \mathbf{w}_o(M_\infty, \alpha) + \delta\mathbf{w}$$
$$\dot{\mathbf{w}}(M_\infty, \alpha) = \dot{\mathbf{w}}_o(M_\infty, \alpha) + \delta\dot{\mathbf{w}}$$
$$\mathbf{x}(M_\infty, \alpha) = \mathbf{x}_o(M_\infty, \alpha) + \delta\mathbf{x}$$
$$\dot{\mathbf{x}}(M_\infty, \alpha) = \dot{\mathbf{x}}_o(M_\infty, \alpha) + \delta\dot{\mathbf{x}}$$

The resulting linearized system is adimensionalized [23] so that it is independent of the freestream density and pressure, and therefore of altitude, but dependent only on the freestream Mach number and angle of attack (assuming a fixed yaw angle). Equation (1) is thus transformed into

$$\bar{\mathbf{A}}_o(\delta\bar{\mathbf{w}})_{,\tau} + \bar{\mathbf{H}}_o\delta\bar{\mathbf{w}} + (\bar{\mathbf{E}}_o + \bar{\mathbf{C}}_o)\delta\dot{\bar{\mathbf{x}}} + \bar{\mathbf{G}}_o\delta\bar{\mathbf{x}} = 0 \tag{4}$$

where

$$\bar{\mathbf{A}}_o = \bar{\mathbf{A}}(\bar{\mathbf{x}}_o) \qquad \bar{\mathbf{H}}_o = \frac{\partial\bar{\mathbf{F}}}{\partial\bar{\mathbf{w}}}(\bar{\mathbf{w}}_o, \bar{\mathbf{x}}_o, \dot{\bar{\mathbf{x}}}_o)$$
$$\bar{\mathbf{E}}_o = \frac{\partial\bar{\mathbf{A}}}{\partial\bar{\mathbf{x}}}(\mathbf{x}_o)\bar{\mathbf{w}}_o \qquad \bar{\mathbf{C}}_o = \frac{\partial\bar{\mathbf{F}}}{\partial\dot{\bar{\mathbf{x}}}}(\bar{\mathbf{w}}_o, \bar{\mathbf{x}}_o, \dot{\bar{\mathbf{x}}}_o)$$
$$\bar{\mathbf{G}}_o = \frac{\partial\bar{\mathbf{F}}}{\partial\bar{\mathbf{x}}}(\bar{\mathbf{w}}_o, \bar{\mathbf{x}}_o, \dot{\bar{\mathbf{x}}}_o)$$

and the bar notation designates adimensionalized quantities. The matrices $\bar{\mathbf{H}}_o$, $\bar{\mathbf{G}}_o$, $\bar{\mathbf{E}}_o$, and $\bar{\mathbf{C}}_o$ are the first-order terms of a Taylor expansion of the adimensionalized numerical flux function around the adimensionalized operating point $(\bar{\mathbf{w}}_o, \bar{\mathbf{x}}_o, \dot{\bar{\mathbf{x}}}_o)$. The matrix $\bar{\mathbf{H}}_o$ has in general a rank equal to the number of fluid degrees of freedom (dof).

The linearization of the structural subsystem is accomplished similarly by perturbing the system in Eq. (2) around an equilibrium state so that

$$\mathbf{u} = \mathbf{w}_o + \delta\mathbf{w}, \qquad \mathbf{u} = \mathbf{u}_o + \delta\mathbf{u}$$
$$\dot{\mathbf{u}} = \dot{\mathbf{u}}_o + \delta\dot{\mathbf{u}}, \qquad \ddot{\mathbf{u}} = \ddot{\mathbf{u}}_o + \delta\ddot{\mathbf{u}}$$

which leads to

$$\mathbf{M}\delta\ddot{\mathbf{u}} + \mathbf{D}_o\delta\dot{\mathbf{u}} + \mathbf{K}_s\delta\mathbf{u} = \mathbf{P}_o\delta\bar{\mathbf{w}} \tag{5}$$

where

$$\mathbf{K}_o = \frac{\partial\mathbf{f}^{\text{int}}}{\partial\mathbf{u}}(\mathbf{u}_o, \dot{\mathbf{u}}_o) \qquad \mathbf{K}_s = \mathbf{K}_o - \frac{\partial\mathbf{f}^{\text{ext}}}{\partial\mathbf{u}}(\mathbf{w}_o, \mathbf{u}_o)$$
$$\mathbf{D}_o = \frac{\partial\mathbf{f}^{\text{int}}}{\partial\dot{\mathbf{u}}}(\mathbf{u}_o, \dot{\mathbf{u}}_o) \qquad \mathbf{P}_o = \frac{\partial\mathbf{f}^{\text{ext}}}{\partial\bar{\mathbf{w}}}(\mathbf{w}_o, \mathbf{u}_o)$$

To keep the notation as compact as possible, the subscript o and the prefix δ are dropped in the remainder of this paper. The same variables $\bar{\mathbf{w}}$, $\bar{\mathbf{x}}$, and $\mathbf{u}$ are used to denote the perturbations of the fluid state, mesh motion, and structural motion vectors, respectively, around the chosen equilibrium point.

The fluid mesh position and velocity variables $\bar{\mathbf{x}}$ and $\dot{\bar{\mathbf{x}}}$ are eliminated from the coupled system of linearized equations by introducing

$$\bar{\mathbf{K}} = \tilde{\mathbf{K}}^{-1}\tilde{\mathbf{K}}_c \tag{6}$$

so that

$$\bar{\mathbf{x}} = \bar{\mathbf{K}}\,\bar{\mathbf{u}} \qquad \dot{\bar{\mathbf{x}}} = \bar{\mathbf{K}}\,\dot{\bar{\mathbf{u}}} \tag{7}$$

where $\bar{\mathbf{u}}$ is measured with respect to its equilibrium configuration. The above algebraic manipulations allow rewriting Eq. (4) as

$$\bar{\mathbf{A}}\bar{\mathbf{w}}_{,\tau} + \bar{\mathbf{H}}\,\bar{\mathbf{w}} + (\bar{\mathbf{E}} + \bar{\mathbf{C}})\bar{\mathbf{K}}\,\dot{\bar{\mathbf{u}}} + \bar{\mathbf{G}}\,\bar{\mathbf{K}}\,\bar{\mathbf{u}} = 0 \tag{8}$$

Next, neglecting the effect of $\partial\mathbf{f}^{\text{ext}}/\partial\mathbf{u}|_o$ and $\mathbf{D}_o$, that is, assuming that $\mathbf{K}_s \approx \mathbf{K}_o$ and zero damping, Eq. (5) is projected on a basis of dry, natural, structural modes and therefore is transformed into

$$\mathbf{I}\,\ddot{\mathbf{u}}_m + \boldsymbol{\Omega}^2\mathbf{u}_m = \mathbf{P}_m\bar{\mathbf{w}} \tag{9}$$

The use of a modal basis to represent the structure accomplishes two important goals. First, it reduces the number of degrees of freedom of the structure, thus contributing to a more compact aeroelastic ROM. Second, it reduces the size of the coupling matrices in the linearized fluid equation (8).

Equations (8) and (9) define the linearized aeroelastic formulation adopted in this paper. Because it depends on the specified freestream Mach number and angle of attack, the linearized fluid subsystem (8) provides a good approximation of its nonlinear counterpart only when perturbed close to its linearization point.

The computational cost associated with the solution of the linearized coupled system of Eqs. (8) and (9) can be expected to be less than that associated with the solution of its nonlinear counterpart; however, this cost can still be considerable because of the size of the discrete fluid subsystem. A POD-based fluid ROM such as the one presented next aims at addressing the latter issue.

B. Construction of POD-Based Fluid and Aeroelastic ROMs

POD is a method that provides a basis for representing a given data set from which a lower-dimensional subspace can be identified. When the given data set is, in some way, representative of a physical system, the resulting reduced basis can be deemed a low-order model of the original full-order model representing that system. The theory and application of POD is covered in many publications [15,35–37]. For the sake of brevity, readers are referred to these references. However, to keep this paper as self-contained as possible, the POD procedure used within the aeroelastic computational framework described in the previous section is summarized here. This procedure is similar in spirit to the approaches exposed in earlier works [10,11].

1) *Generate complex-valued snapshot solutions of Eq. (8) in the frequency domain for various values of the reduced frequency k*:

$$\bar{\mathbf{w}}_j(k) = (ik\bar{\mathbf{A}} + \bar{\mathbf{H}})^{-1}(ik(\bar{\mathbf{E}} + \bar{\mathbf{C}}) + \bar{\mathbf{G}})\bar{\mathbf{K}}\bar{\mathbf{u}}_j \tag{10}$$

Equation (10) is obtained by assuming a periodic solution of the form $\bar{\mathbf{w}} = \bar{\mathbf{w}}_j e^{ik\tau}$ and a periodic excitation of the form $\bar{\mathbf{u}} = \bar{\mathbf{u}}_j e^{ik\tau}$, where $\bar{\mathbf{u}}_j$ is a prescribed structural displacement field. For each specified value of $\bar{\mathbf{u}}_j$, a sweep is performed on the reduced frequency k and several snapshots $\bar{\mathbf{w}}_j(k)$ are generated. Typically, $\bar{\mathbf{u}}_j$ is chosen as a dry natural mode of the structure and therefore the total number of generated snapshots is equal to the product of the number of excitation modes and the number of considered reduced frequencies. The values of k are generated by sweeping over a chosen frequency band. For this purpose, a constant increment Δk is used in this work. Alternatively, a variable Δk can be used to improve the approximation of the correlation matrix $\mathbf{R}$, defined below (see [38] for further details).

2) *Form the real-valued correlation matrix*:

$$\mathbf{R} = \mathbf{S}\mathbf{S}^T \tag{11}$$

where the superscript T designates the transpose,

$$\mathbf{S} = [\text{Re}(\bar{\mathbf{W}}) \quad \text{Im}(\bar{\mathbf{W}})] \tag{12}$$

and each column of $\bar{\mathbf{W}}$ contains a complex-valued snapshot of the form given in Eq. (10).

3) *Compute the eigenvalues and eigenvectors of the correlation matrix* $\mathbf{R}$: However, since all nonzero eigenvalues of the matrix $\mathbf{S}^T\mathbf{S}$ are also eigenvalues of the correlation matrix $\mathbf{R}$, and the size of $\mathbf{S}^T\mathbf{S}$ is significantly smaller than that of $\mathbf{R}$, it is more attractive to replace this step by the solution of the alternative generalized eigenvalue problem $\mathbf{S}^T\mathbf{S}\boldsymbol{\Psi} = \boldsymbol{\Psi}\Lambda$ [31]. Then, form the following POD basis:

$$\boldsymbol{\Phi} = \mathbf{S}\boldsymbol{\Psi}\Lambda^{-\frac{1}{2}} \tag{13}$$

which satisfies

$$\boldsymbol{\Phi}^T\boldsymbol{\Phi} = \mathbf{I} \tag{14}$$

4) *Form a truncated POD basis* $\boldsymbol{\Phi}_r$ *by reducing the size of the matrix* $\boldsymbol{\Phi}$ *to a few r columns*: Usually, the magnitude of the eigenvalue associated with a column of $\boldsymbol{\Psi}$ (and therefore $\boldsymbol{\Phi}$) is used as a criterion for deciding which POD vector to retain and which to discard.

5) *Project the snapshots on the truncated POD basis*:

$$\bar{\mathbf{w}} \approx \boldsymbol{\Phi}_r\bar{\mathbf{w}}_r \leftarrow \bar{\mathbf{w}}_r = \boldsymbol{\Phi}_r^T\bar{\mathbf{w}} \tag{15}$$

6) *Project the governing fluid equation (8) onto the POD basis*: This step leads to

$$(\bar{\mathbf{w}}_r)_{,\tau} = -\boldsymbol{\Phi}_r^T\bar{\mathbf{A}}^{-1}\bar{\mathbf{H}}_r\boldsymbol{\Phi}_r\bar{\mathbf{w}}_r - \boldsymbol{\Phi}_r^T\bar{\mathbf{A}}^{-1}((\bar{\mathbf{E}} + \bar{\mathbf{C}})\bar{\mathbf{K}}\,\dot{\bar{\mathbf{u}}} + \bar{\mathbf{G}}\,\bar{\mathbf{K}}\,\bar{\mathbf{u}}) \tag{16}$$

which is rewritten here as

$$(\bar{\mathbf{w}}_r)_{,\tau} = \bar{\mathbf{H}}_r\bar{\mathbf{w}} - \bar{\mathbf{B}}_r\bar{\mathbf{y}}_r \tag{17}$$

where

$$\bar{\mathbf{H}}_r = -\boldsymbol{\Phi}_r^T(\bar{\mathbf{A}}^{-1}\bar{\mathbf{H}})\boldsymbol{\Phi}_r$$
$$\bar{\mathbf{B}}_r = \boldsymbol{\Phi}_r^T\bar{\mathbf{A}}^{-1}\begin{bmatrix}(\bar{\mathbf{E}} + \bar{\mathbf{C}})\bar{\mathbf{K}} & \bar{\mathbf{G}}\,\bar{\mathbf{K}}\end{bmatrix} \qquad \bar{\mathbf{y}}_r = \begin{bmatrix}\dot{\bar{\mathbf{u}}}\\ \bar{\mathbf{u}}\end{bmatrix} \tag{18}$$

Depending on the size of the truncated POD basis defined in step 4, the adimensionalized reduced-order fluid state vector $\bar{\mathbf{w}}_r$, the fluid subsystem matrix $\bar{\mathbf{H}}_r$, and the coupling matrix $\bar{\mathbf{B}}_r$ can be significantly smaller than their full-order counterparts.

In summary, the POD process outlined previously leads to a reduced basis that can be used for constructing a fluid ROM for a specified freestream Mach number and a specified angle of attack. The corresponding aeroelastic ROM is obtained by coupling Eq. (17) with Eq. (9). The fluid ROM, and therefore the aeroelastic ROM, may be used for computing flows and aeroelastic responses at the specified freestream Mach number and angle of attack, but for variable freestream pressure and density and therefore variable altitude. It is also noted that, although the above procedure can be adapted to generate a POD basis in the time domain, it was observed that ROMs constructed by the frequency domain approach tend to require fewer basis vectors to achieve the desired accuracy [23].

III. Adaptation of the Aeroelastic ROM to Changes in the Mach Number and Angle of Attack

The main drawback of a POD-based ROM such as that described in Sec. II.B—and for that matter, any similarly constructed ROM—is the lack of robustness over an entire parameter space. This is partly because the data samples are collected only within a small region of the state space. Although this focused data sampling leads to a very accurate ROM, it does not lead to a reduced-order basis that can accurately capture the solution space for a wide range of the parameter space. In particular, because the steady-state, adimensionalized fluid solution is a function of the freestream Mach number and angle of attack, the POD basis is sensitive to changes in these two parameters. Thus, a ROM generated by the procedure outlined above cannot be expected to approximate well the fluid subsystem for freestream Mach numbers and/or angles of attack away from the operating (equilibrium) point. To this effect, a few approaches have been proposed to adapt a POD basis to address a parameter variation. These include the GPOD method [39–41], the direct interpolation of the basis vectors [16], and the recently introduced subspace angle interpolation method [16,25,27,28].

The basic idea behind the GPOD approach is to enrich the snapshot matrix $\bar{\mathbf{W}}$ with solutions corresponding to different values of the ROM parameters such as the freestream Mach number and angle of attack. This approach was demonstrated at very low freestream Mach numbers, $0.04 \le M_\infty \le 0.05$, and for angles of attack ranging between 0 and 20 deg. However, besides the fact that, by construction, the GPOD approach loses the optimal approximation property of the POD method, this approach was shown to fail in the transonic regime [23].

As its name suggests, the direct interpolation method generates a POD basis for a new set of model parameters by interpolating the POD basis vectors constructed for previous values of these model parameters. Unfortunately, this simple method was also shown to fail in the transonic regime [16,25].

Alternatively, the subspace angle interpolation method adapts two ROMs associated with two different sets of values of the model parameters to a third set of parameter values, by interpolating the subspace angles between the two given POD bases rather than directly interpolating the vectors of these bases. The basic idea behind this method was introduced in [16]. Preliminary results obtained for its application to full aircraft configurations and changes in the freestream Mach number have recently been reported in [27,28]. In this paper, this method is revisited in the context of adaptation to changes in both the freestream Mach number and angle of attack. New light is shed on its performance in the transonic regime as well as its limitations. Extensive applications to an F-16 aircraft configuration are also presented and discussed.

A. Subspace Angle Interpolation Method

Let n denote the size of the full-order CFD model and $\mathbb{C}$ denote the complex plane.

Definition 1: Let $\mathcal{M}$ denote a subspace of $\mathbb{C}^n$ of dimension p equipped with the usual Hermitian norm, and $\mathcal{N}$ another subspace of $\mathbb{C}^n$ of dimension q with $q \le p$. The smallest angle, $\theta_1 \in [0, \pi/2]$, between $\mathcal{M}$ and $\mathcal{N}$ is defined by

$$\cos\theta_1 = \max_{\substack{\mathbf{u}\in\mathcal{M}\\ \|\mathbf{u}\|_2=1}} \max_{\substack{\mathbf{v}\in\mathcal{N}\\ \|\mathbf{v}\|_2=1}} \mathbf{u}^*\mathbf{v} \tag{19}$$

where $\mathbf{u}$ is not to be confused with its previous meaning, and the * operation denotes the usual Hermitian inner product. Denote by the subscript 1 the pair of vectors $\mathbf{u} \in \mathcal{M}$ and $\mathbf{v} \in \mathcal{N}$ defining θ_1. Each subsequent angle, $\theta_k \in [0, \pi/2]$, $k = 2, \ldots, q$, is defined recursively as the smallest angle between the orthogonal complement in $\mathcal{M}$ to $\{\mathbf{u}_1, \ldots, \mathbf{u}_{k-1}\}$, denoted here by $\mathcal{M}_{k-1}^{\perp}$, and the orthogonal complement in $\mathcal{N}$ to $\{\mathbf{v}_1, \ldots, \mathbf{v}_{k-1}\}$, denoted here by $\mathcal{N}_{k-1}^{\perp}$. This can be written as

$$\cos\theta_k = \left(\max_{\substack{\mathbf{u}\in\mathcal{M}_{\mathbf{k-1}}^{\perp}\\ \|\mathbf{u}\|_2=1}} \max_{\substack{\mathbf{v}\in\mathcal{N}_{\mathbf{k-1}}^{\perp}\\ \|\mathbf{v}\|_2=1}} \mathbf{u}^*\mathbf{v}\right) = \mathbf{u}_k^*\mathbf{v}_k \tag{20}$$

The angles θ_k defined by Eqs. (19) and (20) are known as the principal angles between the subspaces $\mathcal{M}$ and $\mathcal{N}$.

Definition 2: The principal vectors of the pair of subspaces $(\mathcal{M}, \mathcal{N})$ are the two vector sets $\mathbf{U} = \{\mathbf{u}_1, \ldots, \mathbf{u}_q\}$ and $\mathbf{V} = \{\mathbf{v}_1, \ldots, \mathbf{v}_q\}$, where $\mathbf{u}_k$ and $\mathbf{v}_k$ are the vectors introduced in definition 1. $\mathbf{U}$ forms a unitary basis of $\mathcal{M}$, and $\mathbf{V}$ may be complemented by $(p - q)$ unitary vectors to obtain a unitary basis of $\mathcal{N}$.

The principal angles θ_k can be interpreted as the set of angles providing a series of rotations that transform one of the two considered subspaces into the other one. These angles can be computed by the following algorithm [42]. Let $\boldsymbol{\Phi}_1$ and $\boldsymbol{\Phi}_2$ denote two matrices storing the POD basis vectors constructed for two different

values of a model parameter such as the freestream Mach number, and let $\mathbf{Y}$, $\mathbf{\Sigma}$, and $\mathbf{Z}$ be the matrices obtained by the following singular value decomposition (SVD):

$$\mathbf{\Phi}_1^T \mathbf{\Phi}_2 = \mathbf{Y}\mathbf{\Sigma}\mathbf{Z} \tag{21}$$

The cosines of the principal angles θ_k are given by the singular values stored in the diagonal matrix $\mathbf{\Sigma}$, and the principal vectors are given by

$$\mathbf{U} = \mathbf{Y}\mathbf{\Phi}_1 \quad \text{and} \quad \mathbf{V} = \mathbf{Z}\mathbf{\Phi}_2 \tag{22}$$

If for the sake of simplicity $\mathbf{\Phi}_1$ and $\mathbf{\Phi}_2$ have the same size r, the SVD described above yields r principal angles and r pairs of principal vectors.

B. Adaptation to a Change in the Freestream Mach Number

Suppose that two fluid POD bases, $\mathbf{\Phi}_1(M_{\infty_1}, \alpha_1)$ and $\mathbf{\Phi}_2(M_{\infty_2}, \alpha_1)$, corresponding to two different values of the freestream Mach numbers, M_{∞_1} and M_{∞_2}, but the same value of the angle of attack, α_1, have been precomputed. Using this information, the subspace angle interpolation method constructs a fluid POD basis, and then a POD-based aeroelastic ROM, associated with an arbitrary freestream Mach number $M_{\infty_1} < M_\infty < M_{\infty_2}$ in two fast steps. First, it computes the principal angles between $\mathbf{\Phi}_1(M_{\infty_1}, \alpha_1)$ and $\mathbf{\Phi}(M_\infty, \alpha_1)$, $\tilde{\theta}_k$, by linear interpolation as follows:

$$\begin{aligned} &\text{Step 1: } \tilde{\theta}_k(\mathbf{\Phi}_1, \mathbf{\Phi}(M_\infty, \alpha_1)) = \left(\frac{M_\infty - M_{\infty_1}}{M_{\infty_2} - M_{\infty_1}}\right)\theta_k(\mathbf{\Phi}_1, \mathbf{\Phi}_2) \\ &\qquad k = 1, 2, \ldots, r, \qquad M_\infty \in [M_{\infty_1}, M_{\infty_2}] \end{aligned} \tag{23}$$

Then, noting that each principal angle represents the rotation through which a basis vector of one subspace can be transformed into a basis vector of the other subspace, it constructs each vector $\mathbf{e}_k$ of the basis $\mathbf{\Phi}(M_\infty, \alpha_1)$ by rotating the principal vector $\mathbf{u}_k \in \mathbf{U}(M_{\infty_1}, \alpha_1)$ toward its corresponding principal vector $\mathbf{v}_k \in \mathbf{V}(M_{\infty_2}, \alpha_1)$, by an angle equal to the interpolated principal angle $\tilde{\theta}_k(\mathbf{\Phi}_1, \mathbf{\Phi})$ (23) (Fig. 1). Using simple computational geometry, this can be written as

$$\begin{aligned} &\text{Step 2: } \mathbf{e}_k(M_\infty, \alpha_1) = \mathbf{u}_k \cos\tilde{\theta}_k(\mathbf{\Phi}_1, \mathbf{\Phi}) \\ &\quad + \frac{\mathbf{v}_k - (\mathbf{u}_k^T\mathbf{v}_k)\mathbf{u}_k}{\|\mathbf{v}_k - (\mathbf{u}_k^T\mathbf{v}_k)\mathbf{u}_k\|_2}\sin\tilde{\theta}_k(\mathbf{\Phi}_1, \mathbf{\Phi}) \\ &\quad k = 1, 2, \ldots, r \end{aligned} \tag{24}$$

In principle, there exists an infinite number of planes in which the rotation described in step 2 can be performed. The subspace angle interpolation method chooses for this purpose the plane formed by the pair of principal vectors $(\mathbf{u}_k, \mathbf{v}_k)$ to easily satisfy the constraints

$$\mathbf{e}_k(M_{\infty_1}, \alpha_1) = \mathbf{u}_k \quad \text{and} \quad \mathbf{e}_k(M_{\infty_2}, \alpha_1) = \mathbf{v}_k \tag{25}$$

This is equivalent to assuming that the true POD basis vector $\mathbf{e}_k$ lies in the plane formed by the pair of principal vectors $(\mathbf{u}_k, \mathbf{v}_k)$, which may or may not be true.

The set of vectors $\{\mathbf{e}_k\}_{k=1}^{k=r}$ constitutes a fluid POD basis associated with the intermediate freestream Mach number M_∞. Using this basis, Eqs. (9), (17), and (18), the adaptation of the two precomputed aeroelastic ROMs represented by $\mathbf{\Phi}_1$ and $\mathbf{\Phi}_2$ to a change in the freestream Mach number can be performed in near real time on any reasonably fast computing platform. Benefiting applications include, among others, the fast computation of flutter speed index curves.

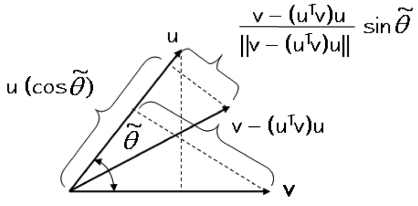

Fig. 1 Rotation of a principal vector u through an interpolated principal angle $\tilde{\theta}$ toward the corresponding principal vector v

C. Adaptation to a Change in the Angle of Attack

Similarly, suppose that two fluid POD bases, $\mathbf{\Phi}_1(M_{\infty_1}, \alpha_1)$ and $\mathbf{\Phi}_2(M_\infty, \alpha_2)$, corresponding to two different values of the angle of attack, α_1 and α_2, but the same value of the freestream Mach number, M_{∞_1}, have been precomputed. Following the same two-step procedure described in the previous section, the subspace angle interpolation method constructs a fluid POD basis, and then a POD-based aeroelastic ROM, associated with an arbitrary angle of attack $\alpha_1 < \alpha < \alpha_2$ as follows. First, it computes the principal angles between $\mathbf{\Phi}_1(M_{\infty_1}, \alpha_1)$ and $\mathbf{\Phi}(M_{\infty_1}, \alpha)$, $\tilde{\theta}_k$, by linear interpolation as follows:

$$\begin{aligned} &\text{Step 1: } \tilde{\theta}_k(\mathbf{\Phi}_1, \mathbf{\Phi}(M_{\infty_1}, \alpha)) = \left(\frac{\alpha - \alpha_1}{\alpha_2 - \alpha_1}\right)\theta_k(\mathbf{\Phi}_1, \mathbf{\Phi}_2) \\ &\qquad k = 1, 2, \ldots, r, \qquad \alpha \in [\alpha_1, \alpha_2] \end{aligned} \tag{26}$$

Then, it constructs each vector $\mathbf{e}_k$ of the basis $\mathbf{\Phi}(M_{\infty_1}, \alpha)$ by rotating the principal vector $\mathbf{u}_k \in \mathbf{U}(M_{\infty_1}, \alpha_1)$ toward its corresponding principal vector $\mathbf{v}_k \in \mathbf{V}(M_{\infty_1}, \alpha_2)$, by an angle equal to the interpolated principal angle $\tilde{\theta}_k(\mathbf{\Phi}_1, \mathbf{\Phi})$ (26). As before, this can be written as

$$\begin{aligned} &\text{Step 2: } \mathbf{e}_k(M_{\infty_1}, \alpha) = \mathbf{u}_k \cos\tilde{\theta}_k(\mathbf{\Phi}_1, \mathbf{\Phi}) \\ &\quad + \frac{\mathbf{v}_k - (\mathbf{u}_k^T\mathbf{v}_k)\mathbf{u}_k}{\|\mathbf{v}_k - (\mathbf{u}_k^T\mathbf{v}_k)\mathbf{u}_k\|_2}\sin\tilde{\theta}_k(\mathbf{\Phi}_1, \mathbf{\Phi}) \\ &\quad k = 1, 2, \ldots, r \end{aligned} \tag{27}$$

Again, using the adapted reduced basis $\mathbf{\Phi}$ described above in the projection steps outlined in Eqs. (9), (17), and (18), the new ROM corresponding to the desired change in the angle of attack can be generated in near real time on any reasonably fast computing platform. Benefiting applications include, among others, the aeroelastic analysis of a system for variable payloads (and therefore variable trim angles).

D. Adaptation to Simultaneous Changes in Freestream Mach Number and Angle of Attack

Both Eqs. (23) and (26) can be interpreted as a first-order Taylor expansion around a given point. This suggests an extension of the subspace angle interpolation method to the case of simultaneous changes in the freestream Mach number and angle of attack whose first step is

$$\begin{aligned} &\text{Step 1}^*\text{: } \tilde{\theta}_k(\mathbf{\Phi}_1(M_{\infty_1}, \alpha_1), \mathbf{\Phi}(M_\infty, \alpha)) \\ &\quad = \left(\frac{M_\infty - M_{\infty_1}}{M_{\infty_2} - M_{\infty_1}}\right)\theta_k(\mathbf{\Phi}_1, \mathbf{\Phi}_2(M_{\infty_2}, \alpha_1)) \\ &\quad + \left(\frac{\alpha - \alpha_1}{\alpha_2 - \alpha_1}\right)\theta_k(\mathbf{\Phi}_1, \mathbf{\Phi}_3(M_{\infty_1}, \alpha_2)) \\ &\quad k = 1, 2, \ldots, r, \qquad M_\infty \in [M_{\infty_1}, M_{\infty_2}], \qquad \alpha \in [\alpha_1, \alpha_2] \end{aligned} \tag{28}$$

and whose second step constructs each vector $\mathbf{e}_k$ of the basis $\mathbf{\Phi}(M_\infty, \alpha)$ by rotating the principal vector $\mathbf{u}_k \in \mathbf{U}(M_{\infty_1}, \alpha_1)$ toward its corresponding principal vector $\mathbf{v}_k \in \mathbf{V}(M_{\infty_2}, \alpha_2)$, by an angle equal to the interpolated principal angle $\tilde{\theta}_k(\mathbf{\Phi}_1, \mathbf{\Phi})$ (26) described previously. This leads to

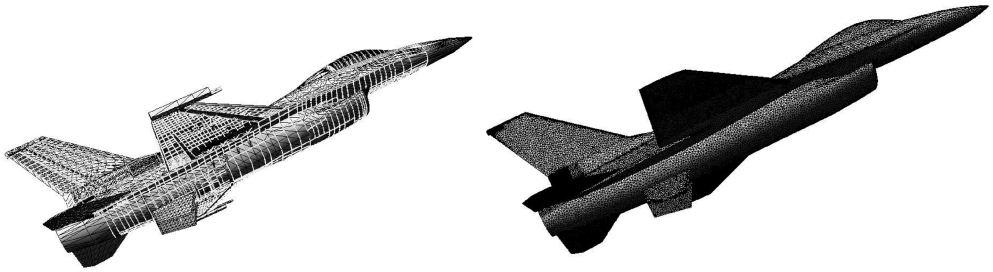

a) Detailed FE structural model b) Fluid surface grid

Fig. 2 F-16 aeroelastic (full-order) computational model.

$$\text{Step 2: } \mathbf{e}_k(M_\infty, \alpha) = \mathbf{u}_k \cos\tilde{\theta}_k(\mathbf{\Phi}_1, \mathbf{\Phi}) + \frac{\mathbf{v}_k - (\mathbf{u}_k^T\mathbf{v}_k)\mathbf{u}_k}{\|\mathbf{v}_k - (\mathbf{u}_k^T\mathbf{v}_k)\mathbf{u}_k\|_2}\sin\tilde{\theta}_k(\mathbf{\Phi}_1, \mathbf{\Phi}) \quad k = 1, 2, \ldots, r \tag{29}$$

Unfortunately, step 1* is difficult to interpret and justify because rotations are usually not additive. Because, in general, the aerodynamics loads vary linearly with the angle of attack but quadratically with the Mach number, the effect of the Mach number is privileged here and the following alternative to step 1* is proposed:

$$\text{Step 1: } \tilde{\theta}_k(\mathbf{\Phi}_1(M_{\infty_1}, \alpha_1), \mathbf{\Phi}(M_\infty, \alpha)) = \left(\frac{M_\infty - M_{\infty_1}}{M_{\infty_2} - M_{\infty_1}}\right)\theta_k(\mathbf{\Phi}_1, \mathbf{\Phi}_2(M_{\infty_2}, \alpha_2)) \quad k = 1, 2, \ldots, r, \qquad M_\infty \in [M_{\infty_1}, M_{\infty_2}] \tag{30}$$

In addition to being more consistent with step 2 described in Eq. (29) where $\mathbf{u}_k \in \mathbf{U}(M_{\infty_1}, \alpha_1)$ and $\mathbf{v}_k \in \mathbf{V}(M_{\infty_2}, \alpha_2)$, step 1 described above has the computational advantage of operating on two rather than three fluid ROMs.

E. Justification and Limitation

As described in the previous sections, the subspace angle interpolation method is essentially a linear approximation method determined by the state of two reference POD subspaces. It can be expected to perform well in the intervals where 1) the principal angles between one of the reference POD subspaces and the sought-after POD subspace vary linearly with the freestream Mach number and/or angle of attack, and 2) the principal vectors of the sought-after POD subspace lie within or close to the plane defined by one corresponding principal vector from each of the reference POD subspaces. This method is particularly interesting when these conditions are satisfied, but the POD basis vectors do not vary linearly with the freestream Mach number and angle of attack in the considered parameter intervals—that is, when the direct basis interpolation method cannot be expected to perform well.

At the time of writing this paper, a drawback of this method is that its extension to higher-order interpolations is unclear. Furthermore, whereas error bounds have been developed for the POD method for nonlinear parabolic systems [43,44], the development of error bounds for the proposed interpolation method remains an open problem. Despite these limitations, the results reported in the remainder of this paper highlight the fact that the subspace angle method offers a significant potential for adapting aeroelastic ROMs to changes in flight parameters as demonstrated next.

IV. Aeroelastic Parametric Identification of a Complete F-16 Configuration

Here, the ROM and ROM adaptation methodologies described in the previous sections are applied to the aeroelastic parametric identification of a complete F-16 configuration with clean wings. The considered full-order aeroelastic computational model consists of a 168,799-dof FE structural model built with bar, beam, solid, plate, and shell, metallic, and composite elements, and an unstructured CFD (Euler) grid with 403,919 vertices and more than 2×10^6 dofs (Fig. 2). This full-order computational model and the AERO code [3,4] are used to generate the various snapshots needed for constructing the aeroelastic ROMs, and to compute full-order linearized as well as nonlinear aeroelastic reference solutions. For each considered freestream Mach number, the trim angle of attack is computed and used to define the flight conditions. In all cases, nine low-frequency dry structural modes are used to construct the aeroelastic ROMs, $\bar{\mathbf{H}}$ is evaluated by a semi-analytical method [30], and $\bar{\mathbf{E}}$, $\bar{\mathbf{C}}$, and $\bar{\mathbf{G}}$ are computed by a finite difference scheme.

First, fixed flight conditions are considered to validate the basic POD-based ROM methodology described in this paper. For this purpose, the lift time histories computed from ROM simulations are compared with their counterparts obtained from full-order computations. In each case, an eigenvalue realization algorithm (ERA) [45] is applied to the simulated lift time histories to extract the aeroelastic damping coefficients. In general, the ERA algorithm requires at least three cycles of time-response data to identify a mode. For fighter aircraft, the first torsional mode usually plays an important role in flutter. For the F-16 aircraft configuration considered here, the frequency of the first dry torsional mode is about 7.4 Hz. This means that the identification by the chosen ERA of the aeroelastic damping coefficient of the first torsional mode requires the simulation of the first 0.5 s of aeroelastic response of the considered F-16 aircraft configuration. However, to increase the level of confidence in the identification procedure, the time-domain simulations are performed in most cases for a time window of 0.75 s. The results obtained using the aeroelastic ROMs and full-order model counterparts are contrasted and compared with the results obtained from flight test data.

Next, both the subspace angle and direct basis interpolation methods are applied to adapt the ROMs constructed for fixed flight conditions to various changes in the freestream Mach number and angle of attack. Again, lift histories and aeroelastic damping ratios are reported to analyze and contrast the performances of these two adaptation methods.

All computations are performed on a Linux cluster with 32 Pentium 4, 3.0 GHz processors. CPU performance results are reported for all ROM-based, adapted ROM-based, and full-order nonlinear simulations.

A. ROM Validation for Fixed Freestream Mach Number and Angle of Attack

Here, POD-based ROMs of the F-16 fighter are constructed for fixed flight conditions. First, the freestream Mach number is set to $M_\infty = 0.799$, and the angle of attack is set to the corresponding trim value $\alpha = 2.4$ deg. Snapshots are generated by applying an excitation that is proportional to a particular structural mode for five different values of the reduced frequency $0 \leq k \leq 0.02$. The snapshot collection process is repeated for nine different dry modes of the structural model. An aeroelastic ROM is then constructed following the procedure outlined in Sec. II.B. The performance of this ROM is assessed by applying it to the prediction of the transient aeroelastic response to a disturbance of the trimmed aircraft at

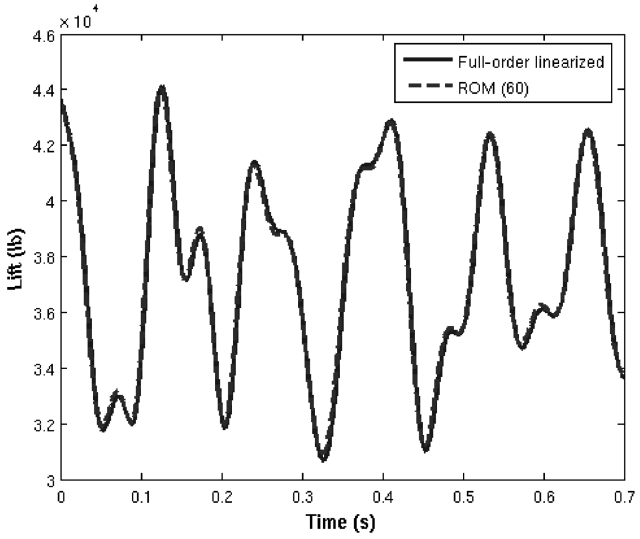

a) $q_\infty = 650$ *lb/ft*^{2}, $h = 10{,}000$ *ft*

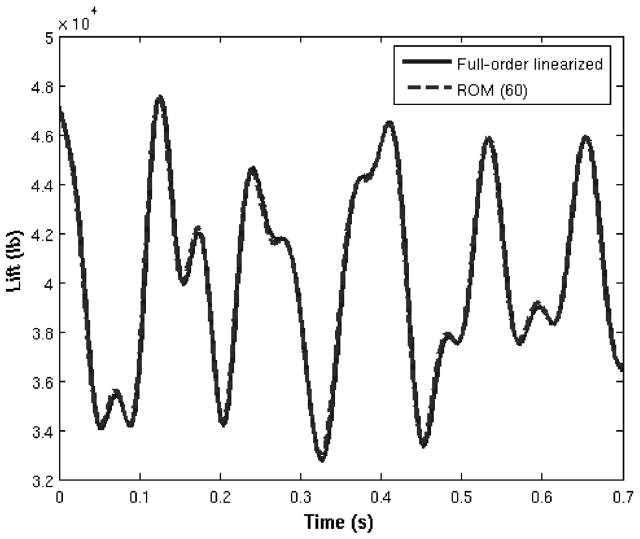

b) $q_\infty = 703$ *lb/ft*^{2}, $h = 8{,}000$ *ft*

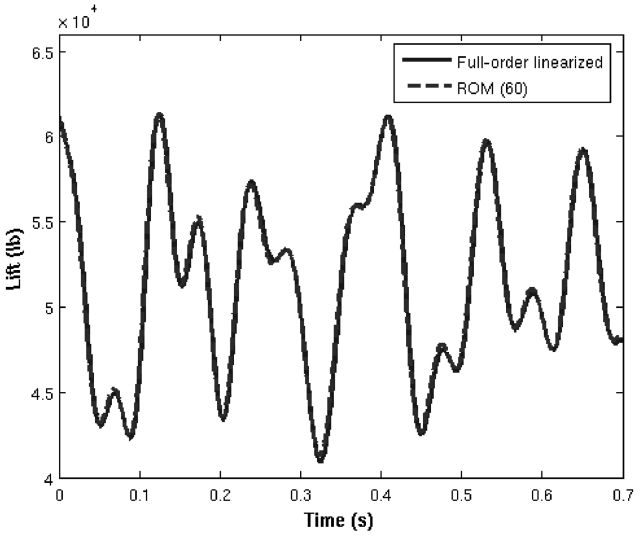

c) $q_\infty = 912$ *lb/ft*^{2}, $h = 1{,}000$ *ft*

Fig. 3 Lift time histories generated for $M_\infty = 0.799$ and various freestream dynamic pressures q_∞, using i) the aeroelastic ROM, and ii) the full-order linearized fluid model coupled with the modalized structural model.

various altitudes. The disturbance is generated by an initial displacement excitation proportional to the first dry torsional mode. Figure 3 reports, for various values of the freestream dynamic pressure, the lift time histories predicted using the constructed ROM, and an aeroelastic model in which the full-order linearized fluid model is coupled to the modalized structure. The number of POD basis vectors used in the ROM construction is identified between parentheses in all figure legends. The reader can observe that in all cases, the ROM performs well. Figure 4 focuses on the freestream dynamic pressure $q_\infty = 650$ lb/ft^2 at 10,000 ft altitude and compares the time history of the lift predicted by the ROM with that predicted by the full-order nonlinear aeroelastic model. The reader can observe that the ROM is capable of tracking well the full-order nonlinear aeroelastic solution. Both lift time histories exhibit the same frequency, but very minor variations in amplitude.

Next, several other aeroelastic ROMs are constructed using the same procedure outlined previously for subsonic, transonic, and supersonic trimmed flight conditions. The lift time histories are generated and postprocessed by the ERA to compute the aeroelastic damping coefficients of the first torsional mode. The results are reported in Fig. 5 as a function of the freestream Mach number, and compared with their counterparts obtained from full-order nonlinear simulations and flight test data. Given all the uncertainties associated

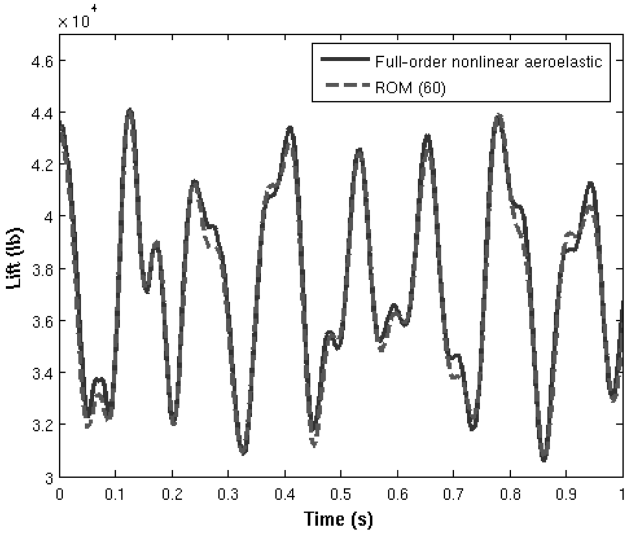

Fig. 4 Comparison between the lift time histories predicted by i) the aeroelastic ROM, and ii) the full-order nonlinear aeroelastic model.

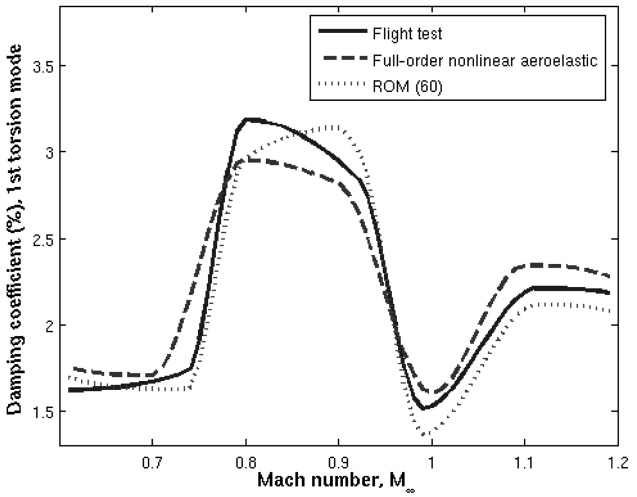

Fig. 5 Variation with the freestream Mach number of the damping ratio associated with the first torsional mode: comparison between the results generated by i) the ROM, ii) full-order nonlinear simulations, and iii) counterparts obtained from flight test data.

with this problem, the observed agreement between the aeroelastic damping coefficients predicted by the ROM-based simulations and the full-order nonlinear simulations, and those obtained from flight test data, is considered to be good.

B. ROM Adaptation to Changes in Flight Conditions

1. Adaptation to Changes in Freestream Mach Number

First, the potential of the subspace angle interpolation method for adapting ROMs to changes in the freestream Mach number is illustrated. To this effect, two POD bases are precomputed at two different freestream Mach numbers, $M_{\infty_1} = 0.611$ and $M_{\infty_2} = 0.799$, but a fixed angle of attack $\alpha_1 = 0$ deg. Then, both the subspace angle and the direct basis interpolation methods are applied to the adaptation of these two ROMs to the new freestream Mach number $M_\infty = 0.710$, while maintaining the same angle of attack $\alpha_1 = 0$ deg. Finally, an implicit time integrator is applied to the two ROMs produced by the two aforementioned interpolation methods to predict the transient aeroelastic response of the F-16 to a disturbance around the new flight condition ($M_\infty = 0.710$, $\alpha_1 = 0$ deg).

Figure 6 reports the lift time history produced by the Mach-adapted ROM using the subspace angle interpolation method. It also compares it with that obtained by coupling the modalized structure with the CFD-based full-order fluid model linearized around $M_\infty = 0.710$. The computed lift histories have the same dominant frequency. However, the lift response produced by the ROM adapted by the subspace iteration method exhibits a moderate amplitude error.

On the other hand, the direct basis interpolation method fails to generate a stable ROM in this case. Indeed, Fig. 7 shows that even when a very small time step is used, and two different sizes of the adapted ROM are considered, the computation of the lift time history diverges.

At least for this problem, the failure of the direct linear basis interpolation approach and the success of the subspace angle linear interpolation method can be explained by examining the variation of the quantity they interpolate with the freestream Mach number. Indeed, Fig. 8 shows that within the considered Mach range, the subspace angle varies linearly with the freestream Mach number, but at least one component of the POD vectors exhibits a nonlinear variation with M_∞. Hence, it is not surprising that, at least for this problem, the subspace angle interpolation method produces a reasonably accurate Mach-adapted ROM, whereas the direct basis interpolation method does not. It is also noted that earlier studies [16] have furthermore shown that even higher-order interpolations do not improve the accuracy of the direct basis interpolation approach.

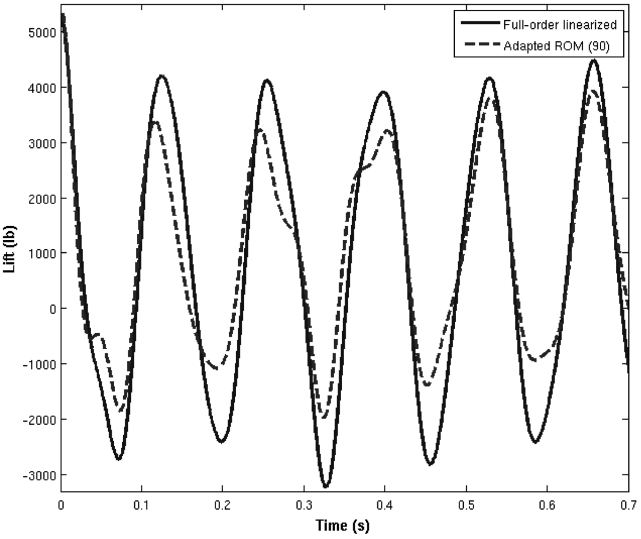

Fig. 6 Comparison between the lift time histories generated by i) adapting the two ROMs constructed at ($M_{\infty_1} = 0.611$, $\alpha_1 = 0$ deg) and ($M_{\infty_2} = 0.799$, α_1) to ($M_\infty = 0.710$, α_1) using the subspace angle interpolation method, and ii) coupling the full-order fluid model linearized at ($M_\infty = 0.710$, α_1) with the modalized structure.

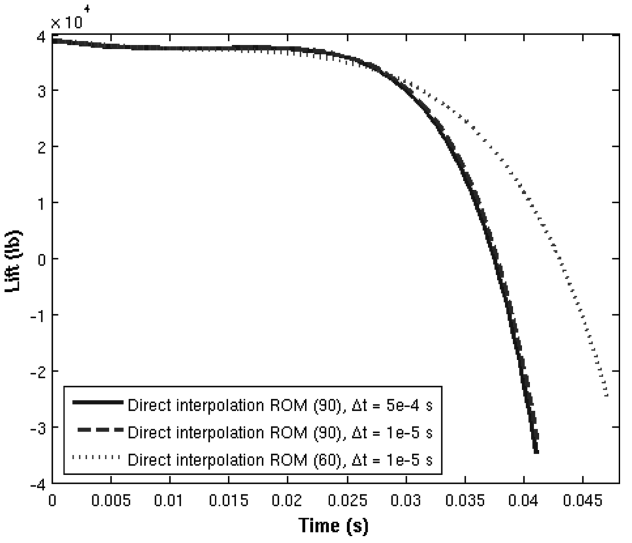

Fig. 7 Lift time histories generated by adapting the two ROMs constructed at ($M_{\infty_1} = 0.611$, $\alpha_1 = 4.5$ deg) and ($M_{\infty_2} = 0.799$, α_1) to ($M_\infty = 0.710$, α_1) using the direct basis interpolation method: effect of the computational time step Δt and the number of POD basis vectors (shown between parentheses).

2. Adaptation to Changes in Angle of Attack

Next, the freestream Mach number is set to $M_{\infty_1} = 0.799$, and the potential of the subspace angle interpolation method for adapting ROMs to changes in the angle of attack is examined. More specifically, two ROMs are assumed to have been precomputed at two different angles of attack, α_1 and α_2, and the objective is set to adapt these two ROMs to a new angle of attack α, with $\alpha_1 < \alpha < \alpha_2$. First, α is set to $\alpha = 2.7$ deg, and various bracketing pairs (α_1, α_2) are considered. Figure 9 reports the lift time histories obtained using the ROMs computed by the subspace angle and direct basis interpolation methods, respectively, and compares them with the result of a corresponding full-order linearized aeroelastic simulation. Both interpolation methods are shown to perform well when the distance between the two bracketing angles of attack $\Delta\alpha = |\alpha_2 - \alpha_1|$ is relatively small. When $\Delta\alpha$ is increased, the accuracy of both interpolation methods is decreased. However, the subspace angle interpolation method is shown to be more robust than the direct basis

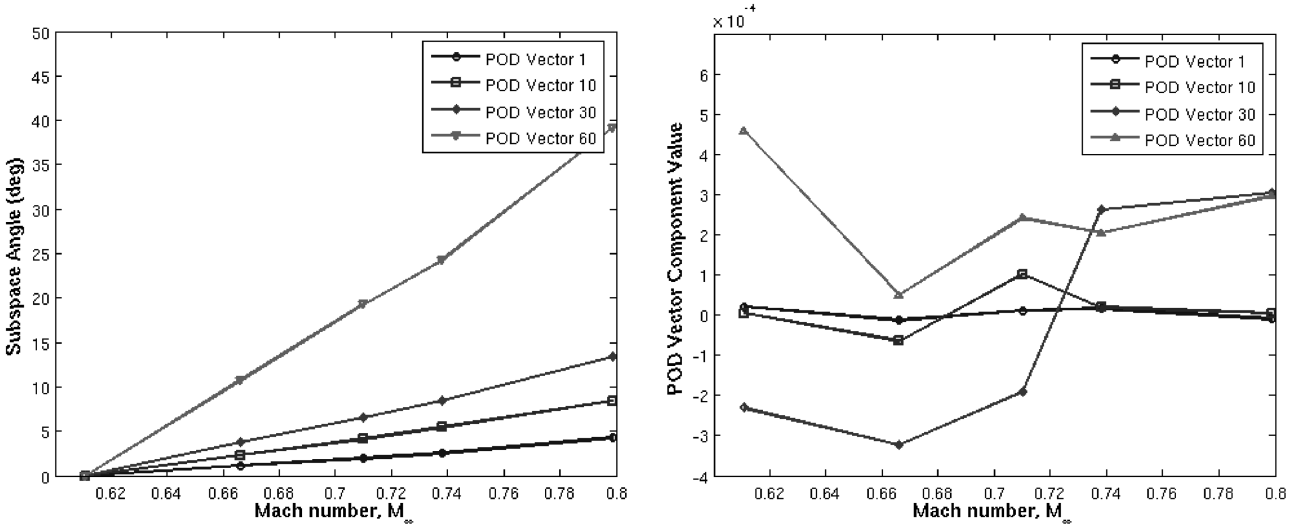

a) Variation of the POD subspace angles

b) Variation of the POD vector component values

Fig. 8 Variation of the true subspace angles and true POD basis vectors (one component) with the Mach number.

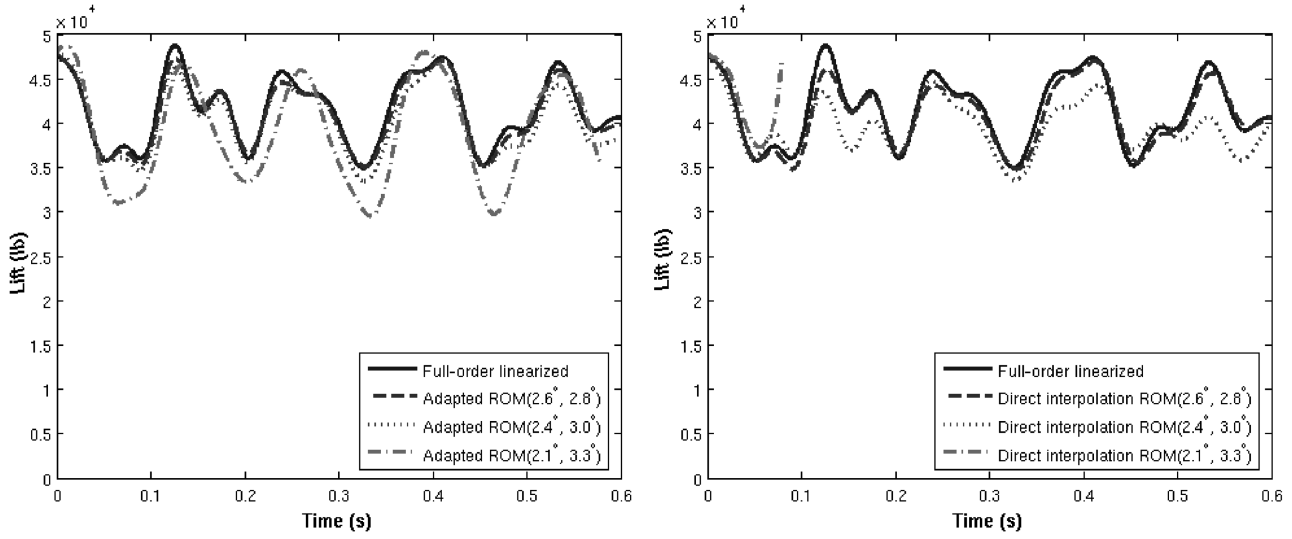

a) Subspace angle interpolation

b) Basis interpolation

Fig. 9 Comparison of the lift time histories generated for the flight conditions ($M_{\infty_1} = 0.799, \alpha = 2.7$ deg) using i) the ROM obtained by adaptation to $\alpha = 2.7$ deg of the two ROMs constructed at $M_{\infty_1} = 0.799$ and the two different angles of attack specified between parentheses; ii) the full-order linearized model.

interpolation method. For example, when the distance between the two bracketing angles of attack is as large as $\Delta\alpha = 1.2$ deg, the direct interpolation method fails to generate a stable ROM. On the other hand, the subspace angle method produces a stable ROM in each considered case.

Next, the damping coefficients are extracted for the first torsional aeroelastic mode from the lift time histories generated using the full-order linearized model, as well as the angle of attack-adapted ROMs. The results are summarized in Table 1. Both the subspace angle and direct basis interpolation methods are reported to produce reasonably accurate results. The subspace angle iteration method is also shown to be slightly more accurate than the direct basis interpolation approach. For the largest interpolation window, the ERA software failed to perform the identification.

To explain the limited angle of attack parameter space for which the subspace angle interpolation method is able to perform a viable ROM adaptation, the variations of the true subspace angles with the angle of attack are plotted in Fig. 10. A linear trend is observed over a large range of angles of attack. Nevertheless, as discussed above, the subspace angle linear interpolation method does not perform well over this entire range of angles of attack. Therefore, it is conjectured that when this happens, the reason is that the true POD basis vectors lie far outside the plane defined by the POD principal basis vectors used to perform the adaptation, which invalidates the assumption behind Eq. (29) that was stated in Sec. III.B. To verify this conjecture, the POD basis is reconstructed at $\alpha = 2.7$ deg. Then, the subspace angles formed by this POD basis and the POD basis constructed at $\alpha_{\text{ref}} = 2.4$ deg (chosen here as the reference POD basis) are compared with the subspace angles formed between the POD basis obtained by adaptation to $\alpha = 2.7$ deg of the ROMs precomputed at $\alpha_1 = 2.1$ deg and $\alpha_2 = 3.3$ deg, and the reference POD basis. The results are reported in Fig. 11. As expected, they reveal that the subspace angle method performs a reasonably accurate interpolation. However, Fig. 12 reports that for the bracketing angles of attack $\alpha_1 = 2.1$ deg and $\alpha_2 = 3.3$ deg, the reconstructed and adapted POD bases have large subspace angles between their higher principal vectors, which indicates that the exact POD vectors at the new angle of attack lie in fact far outside the planes formed by the POD principal

Table 1 Aeroelastic damping coefficients computed for ($M_{\infty_1} = 0.799$ deg, $\alpha = 2.7$ deg) using 1) the ROM obtained by adaptation of two ROMs constructed at $M_{\infty_1} = 0.7999$ and the two angles of attack specified between parentheses, and 2) the full-order linearized model

Aeroelastic computational model	First torsional aeroelastic damping ratio, %	Relative error, %
Full-order linearized	3.02	Reference
Subspace angle interpolated ROM (2.6, 2.8 deg)	2.85	−5.6
Direct basis interpolated ROM (2.6, 2.8 deg)	2.80	−7.3
Subspace angle interpolated ROM (2.4, 3.0 deg)	3.18	5.3
Direct basis interpolated ROM (2.4, 3.0 deg)	2.82	−6.6
Subspace angle interpolated ROM (2.1, 3.3 deg)	Not identifiable	N/A
Direct basis interpolated ROM (2.1, 3.3 deg)	Not identifiable	N/A

basis vectors used in the adaptation procedure. On the other hand, when the narrower bracketing range of angles of attack ($\alpha_1 = 2.6$ deg, $\alpha_2 = 2.8$ deg) is used, the adapted basis is reported to converge reasonably well toward the exact basis.

3. *Adaptation to Simultaneous Changes in Freestream Mach Number and Angle of Attack*

Finally, this section demonstrates the potential of the subspace angle iteration method for adapting aeroelastic ROMs to simultaneous changes in both the freestream Mach number and the angle of attack. These typically occur when considering trimmed flight conditions at various speeds.

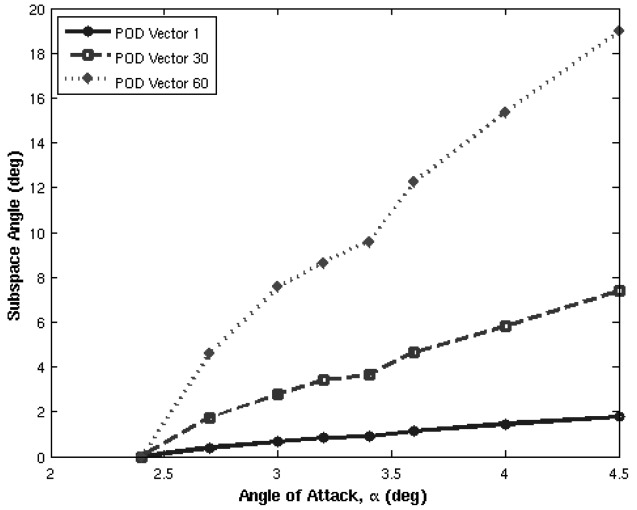

Fig. 10 Variation with the angle of attack of the POD subspace angles.

First, two POD bases are precomputed at two different trimmed flight conditions ($M_{\infty_1} = 0.611, \alpha_1 = 4.5$ deg), and ($M_{\infty_2} = 0.799$, $\alpha_2 = 2.4$ deg). Then, the subspace angle iteration method is applied to continuously adapt these two ROMs to generate in near real time a suite of trimmed aeroelastic ROMs associated with $0.611 \leq M_\infty \leq 0.799$. To evaluate their suitability for flutter analysis, these ROMs are then used to generate transient aeroelastic responses to various disturbances. As before, the ERA software is applied to extract from these time responses the aeroelastic damping coefficients of the first torsional mode of the F-16 aircraft at various trimmed configurations. Because flight test data are not available to the authors in this specific range of the freestream Mach number, the resulting numerical predictions are compared in Fig. 13 with their counterparts obtained from full-order nonlinear aeroelastic simulations. The reader can observe that, at least for this problem, the subspace angle iteration method performs well at adapting aeroelastic ROMs to simultaneous changes in the freestream Mach number and angle of attack.

Next, the subspace angle interpolation method is applied to a Mach number range in the transonic-to-early-supersonic regime. To this effect, two POD bases are precomputed at the trimmed flight conditions ($M_{\infty_1} = 0.923$, $\alpha_1 = 1.4$ deg) and ($M_{\infty_2} = 1.114$, $\alpha_2 = 1.5$ deg). Then, these two ROMs are continuously adapted to $0.923 \leq M_\infty \leq 1.114$ and the corresponding trim angles of attack. In this case, it turns out that the subspace angle linear interpolation method fails to generate a stable adapted ROM at each of the two operating points $M_\infty = 1.072$ and $M_\infty = 1.031$. This is illustrated in Fig. 14 which focuses on the lift time histories associated with the prediction of the transient aeroelastic responses to disturbances using these two adapted ROMs. Figure 15 suggests that the reason behind

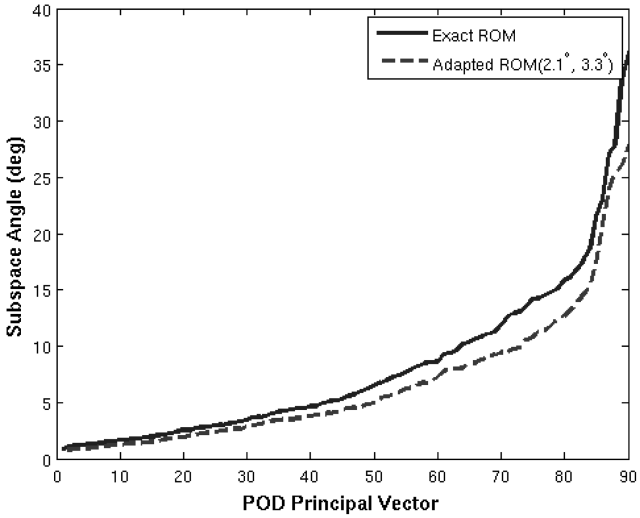

Fig. 11 Comparison of the exact and interpolated subspace angles ($M_{\infty_1} = 0.799, \alpha = 2.7$ deg).

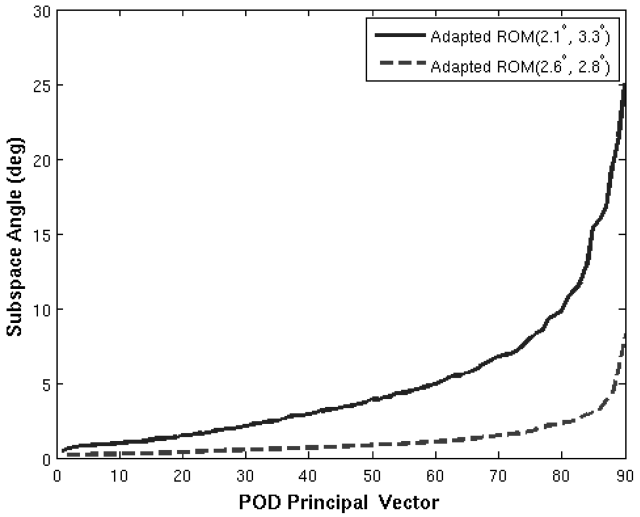

Fig. 12 Subspace angles between the exact POD subspace and various angle of attack-adapted POD subspaces ($M_{\infty_1} = 0.799, \alpha = 2.7$ deg).

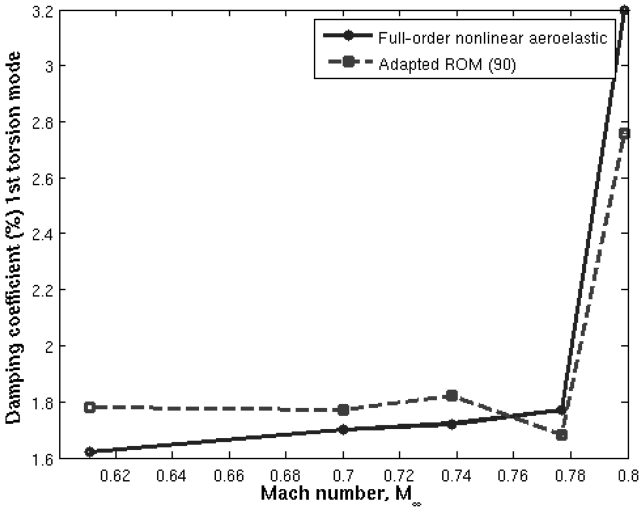

Fig. 13 Comparison of the first aeroelastic torsional damping coefficients generated by i) continuously adapting the two ROMs constructed at ($M_{\infty_1} = 0.611$, $\alpha_1 = 4.5$ deg) and ($M_{\infty_2} = 0.799$, $\alpha_2 = 2.4$ deg) to the new, continuously trimmed flight conditions ($0.611 \leq M_\infty \leq 0.799$, α_{trim}), and ii) full-order nonlinear simulations.

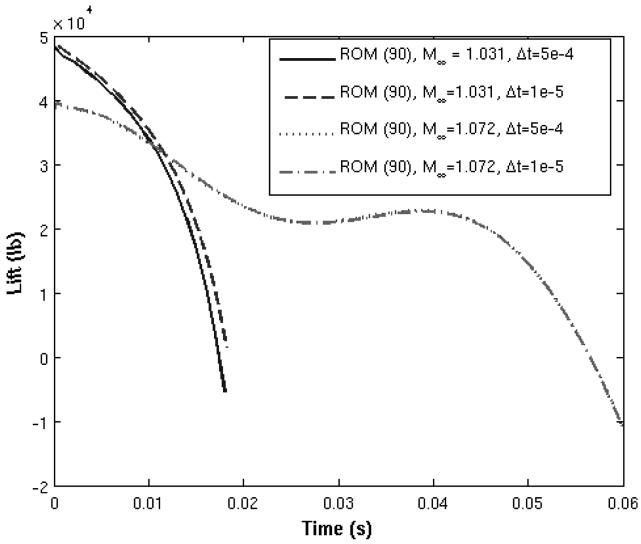

Fig. 14 Unstable lift time histories predicted by adapting the two ROMs precomputed at the trimmed flight conditions ($M_{\infty_1} = 0.923$, $\alpha_1 = 1.4$ deg) and ($M_{\infty_2} = 1.114$, $\alpha_2 = 1.5$ deg) to the two new trimmed flight conditions ($M_\infty = 1.031$, $\alpha = 1.4$ deg) and ($M_\infty = 1.072$, $\alpha = 1.45$ deg) using the subspace angle interpolation method.

this failure in this case is most likely due to the nonlinear variation of the subspace angles associated with the higher principal vectors within the specified range of trimmed flight conditions. To resolve this issue, an intermediate data point is introduced: a third POD basis is precomputed at $M_{\infty_3} = 1.031$ and its trim angle of attack $\alpha_3 = 1.4$ deg. Figure 16 reveals that using this POD basis and that precomputed at ($M_{\infty_2} = 1.114$, $\alpha_2 = 1.5$ deg), the subspace angle interpolation method produces an adapted ROM that tracks well the lift time history predicted by the full-order nonlinear simulation at $M_\infty = 1.072$. Hence, the given problem is repeated and the subspace angle interpolation method is applied this time to the piecewise adaptation of the three precomputed ROMs described above to $0.923 \leq M_\infty \leq 1.114$ and the corresponding trim angles of attack. Figure 17 reports the first torsional aeroelastic damping coefficients obtained with the adapted ROMs and compares them with their counterparts from full-order nonlinear simulations. With the exception of the case $M_\infty = 0.990$, the interpolated ROMs are

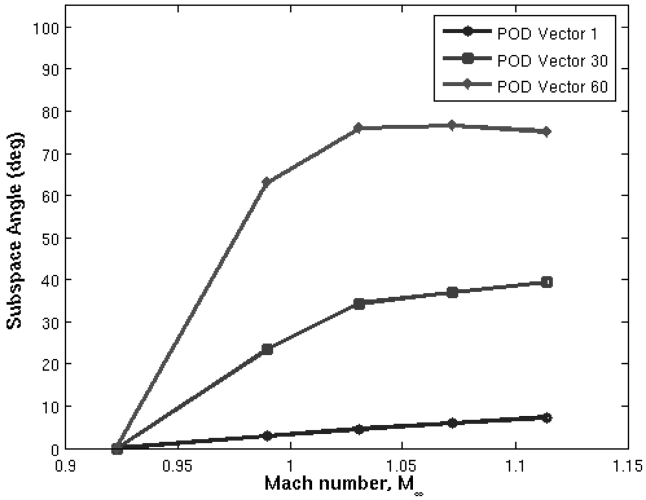

Fig. 15 Variation of the true POD subspace angles with the trimmed flight conditions.

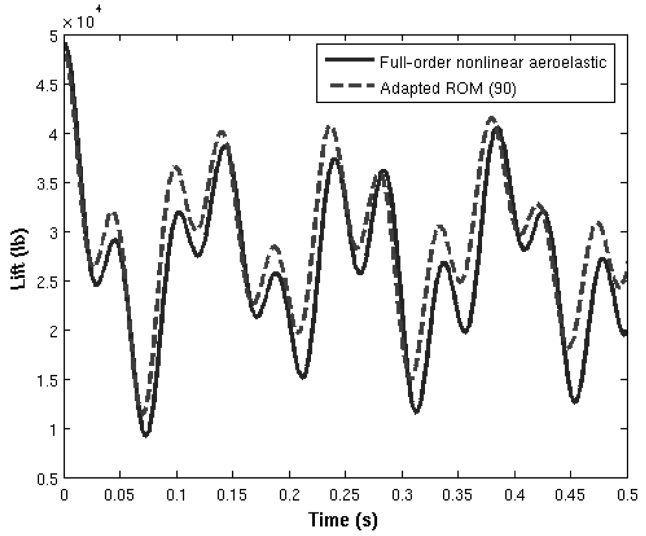

Fig. 16 Comparison of the lift time histories generated by i) adapting the two ROMs constructed at the trimmed flight conditions ($M_{\infty_1} = 1.031$, $\alpha_1 = 1.4$ deg) and ($M_{\infty_2} = 1.114$, $\alpha_2 = 1.5$ deg) to the new trimmed operating point ($M_\infty = 1.072$, $\alpha = 1.45$ deg) using the subspace angle method, and ii) the full-order nonlinear aeroelastic simulation.

shown to track relatively well the variation of the aeroelastic damping ratio with the freestream Mach number.

C. Computational Cost

Table 2 summarizes the details of the CPU cost associated with constructing on 32 processors the fluid ROM at ($M_\infty = 0.799$, $\alpha = 2.4$ deg) for the given F-16 aircraft configuration, using the computational infrastructure described at the beginning of Sec. IV. As it can be expected, the CPU time elapsed in the generation of the computational snapshots accounts for the vast majority of the computational cost. For comparison, Table 3 reports the CPU cost associated with the prediction of the first 0.75 s of the transient aeroelastic response of this aircraft to a disturbance using the various full-order computational models, as well as the precomputed reduced-order model. From these performance results, and the fact that the CPU cost of a nonlinear aeroelastic simulation scales almost linearly with the size of the time window to be covered by the simulation, it follows that the construction of an aeroelastic ROM and its subsequent exploitation for a time-domain aeroelastic simulation is computationally more efficient than the comparable

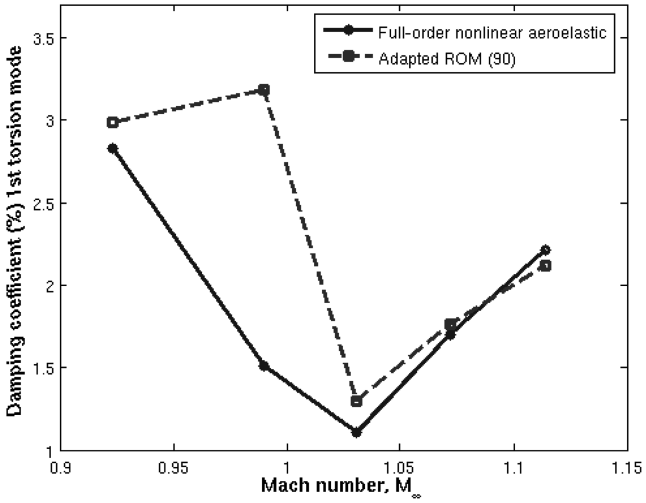

Fig. 17 Comparison of the torsional aeroelastic damping coefficients generated by i) piecewise adapting the three ROMs constructed at the three trimmed flight conditions ($M_{\infty_1} = 0.923$, $\alpha_1 = 1.4$ deg), ($M_{\infty_2} = 1.031$, $\alpha_2 = 1.4$ deg), and ($M_{\infty_3} = 1.114$, $\alpha_3 = 1.5$ deg) to the new, continuously trimmed operating points ($0.923 \leq M_\infty \leq 1.114$, α_{trim}) using the subspace angle interpolation method, and ii) full-order nonlinear simulations.

full-order nonlinear aeroelastic simulation, when the time window is greater or equal to 0.39 s, that is, about 3 times the period of the first dry torsional mode of this aircraft. For shorter-term simulations, the construction and exploitation of the aeroelastic ROM becomes more computationally intensive than the corresponding full-order nonlinear aeroelastic simulation. Therefore, for a single flight condition and time-domain computations, a CFD-based ROM technology such as the one described in this paper is attractive mostly for long-term simulations (for a discussion of related eigencomputations, see [30,34] and references cited therein).

Table 2 CPU cost on 32 processors of the construction of the fluid ROM at ($M_\infty = 0.799$, $\alpha = 2.4$ deg, complete F-16 configuration)

Snapshot interval	$\Delta k = 0.004$
Total number of snapshots	99
CPU time elapsed in snapshot generation	10,944 s (3.04 h)
CPU time elapsed in POD basis construction	10 s
CPU time elapsed in matrix projections	108 s (0.03 h)
Total CPU time elapsed in ROM construction	11,062 s (3.07 h)

Table 3 CPU cost associated with the aeroelastic simulation of the first 0.75 s of the transient aeroelastic response of the F-16 aircraft configuration using various computational models ($M_\infty = 0.799$, $\alpha = 2.4$ deg)

Aeroelastic computational model	No. of processors	CPU time
Full-order, nonlinear	32	21,168 s (5.88 h)
Full-order, linearized fluid coupled with modalized structure	32	2880 s (0.80 h)
Precomputed, reduced-order (ROM)	1	72 s (0.02 h)

As is often the case with ROMs, the computational efficiency of the CFD-based aeroelastic ROM technology described in this paper depends on the number of opportunities for reusing a computed aeroelastic ROM. Because the underlying fluid ROM is computed at a given freestream Mach number and a given angle of attack, the opportunities for reusing it are not as numerous as often implied in the aeroelastic literature (except perhaps for some control applications). For flutter analysis, the typical sweep procedure fixes the freestream Mach number and finds or clears flutter at this point by varying the freestream density or pressure. Usually, this takes about five iterations. Therefore, a fixed-parameter ROM technology has the potential of reducing the computational cost of such a flutter analysis by approximately a factor of 5. However, in design analysis or limit cycle oscillation detection, other parameters related to the structure such as stiffness, mass, and damping are often varied. In such cases, the aerodynamic ROM may also be reused or quickly recomputed [15] using additional snapshots, thus offering increased computational savings proportional to the number of desired analyses which can be on the order of hundreds. This is a significant improvement for certain applications, but insufficient for enabling routine, CFD-based, aeroelastic analyses under varying aerodynamic conditions in design and test operations. The reader can also note that the performance results reported in Tables 2 and 3 suggest that under the same circumstances, the full-order linearized aeroelastic computational technology offers the same if not better speedup factor than the CFD-based ROM technology. All this underscores the need for a successful methodology for adapting in near real time CFD-based ROMs to new trimmed flight conditions.

Table 4 reports the computational costs associated with the identification on 32 processors of the aeroelastic first torsion damping ratios in the subsonic Mach range [0.611, 0.799] and transonic Mach range [0.923, 1.114] discussed in Sec. IV.B, using the full-order nonlinear and adapted ROM F-16 computational models. These results suggest that the subspace angle interpolation method is a good step toward the objective stated above. Indeed, when applied to the adaptation to a new freestream Mach number and a new angle of attack of any two of the precomputed F-16 ROMs, it consumes only 2 min of CPU time. As a result, it speeds up the aforementioned parametric identification of the F-16 aircraft, with respect to full-order nonlinear aeroelastic simulations, by a factor of the order of 16 in the subsonic regime, when the Mach range [0.611, 0.799] is sampled into 19 different trimmed flight conditions. This speedup factor is of the order of 10 in the transonic case, when the Mach range [0.923, 1.114] is sampled into 23 different trimmed flight conditions. The difference in computational efficiency between the subsonic and transonic cases is due to the use of four rather than two precomputed ROMs in the Mach range [0.923, 1.114] to fix the inaccuracy at $M_\infty = 0.990$ observed in Fig. 17.

V. Conclusions

There are three important facts to keep in mind when considering a CFD-based aeroelastic ROM for aircraft applications: 1) a computational aeroelastic ROM is typically constructed at a given freestream Mach number M_∞ and given angle of attack α, 2) its construction can be CPU intensive, and 3) once constructed, it lacks robustness with respect to changes in M_∞ and α. Hence, to enable routine aeroelastic numerical simulations in design, analysis, and test operations, a ROM-based computational technology should include

Table 4 Identification of the aeroelastic first torsion damping ratios of the F-16 fighter: comparative CPU costs on 32 processors of 1) full-order nonlinear simulations, and 2) adapted-ROM simulations

Mach range	ΔM_∞	N_{tfc}[a]	Total CPU full-order nonlinear simulations	Total CPU adapted ROM simulations	CPU ROM generation	CPU ROM adaptation (SAIM)[b]	CPU[c] response analysis
0.611–0.799	0.1	19	111.72 h	7.09 h	6.14 h (3.07 h/ROM)	0.57 h (2 min /ROM)	0.38 h
0.923–1.114	0.01	23	135.24 h	13.37 h	12.28 h	0.63 h	0.46 h

[a] N_{tfc} = no. of trimmed flight conditions.
[b] SAIM = subspace angle interpolation method.
[c] Serial execution (on a single processor).

a means for rapidly adapting a precomputed ROM to different freestream Mach numbers and different angles of attack. When the fluid ROM is based on the proper orthogonal decomposition method, the following results are consistently observed for verified and validated aeroelastic computations performed on an F-16 clean wing configuration. Interpolating the basis vectors of two bracketing ROMs is not a good adaptation algorithm because these vectors vary nonlinearly with M_∞ and α within any reasonable interval for each of these two parameters. On the other hand, the principal angles between the subspaces of two bracketing ROMs appear to vary linearly within reasonably large intervals of a given subsonic freestream Mach number, say [0.6, 0.8], but intervals half this size in the transonic regime. For this reason, the subspace angle *linear* interpolation method, which was refined in this paper to address simultaneous changes in both the freestream Mach number and angle of attack, succeeds at adapting aeroelastic ROMs to different *trimmed* flight conditions for problems where the direct interpolation of the ROM basis vectors fails to do so. Furthermore, it completes the ROM adaptation in an amount of CPU time that is 2 orders of magnitude smaller than that required for constructing one ROM. However, realizing the full potential of the subspace angle interpolation method requires extending it to higher-order interpolation schemes, a goal that is currently pursued by the authors of this paper.

Acknowledgments

This material is based upon work supported partially by the U.S. Air Force Office of Scientific Research under Grant F49620-01-1-0129, and partially by the National Science Foundation under Grant CNS-0540419.

References

[1] Sadeghi, M., and Liu, F., "Investigation of Non-Linear Flutter by a Coupled Aerodynamics and Structural Dynamics Method," AIAA Paper 2001-0573, 2001.

[2] Liu, F., Cai, J., and Zhu, Y., "Calculation of Wing Flutter by a Coupled Fluid-Structure Method," *Journal of Aircraft*, Vol. 38, No. 2, 2001, pp. 334–342.

[3] Geuzaine, P., Brown, G., Harris, C., and Farhat, C., "Aeroelastic Dynamic Anlysis of a Full F-16 Configuration for Various Flight Conditions," *AIAA Journal*, Vol. 41, No. 3, 2003, pp. 363–371.

[4] Farhat, C., Geuzaine, P., and Brown, G., "Application of a Three-Field Nonlinear Fluid-Structure Formulation to the Prediction of the Aeroelastic Parameters of an F-16 Fighter," *Computers and Fluids*, Vol. 32, No. 1, 2003, pp. 3–29.

[5] Ashley, H., and Zartarian, G., "Piston Theory—A New Aerodynamic Tool for the Aeroelastician," *Journal of Aerospace Sciences*, Vol. 23, No. 12, 1956, pp. 1109–1118.

[6] Albano, E., and Rodden, W., "A Doublet-Lattice Method for Calculating Lift Distribution on Oscillating Surfaces in Subsonic Flow," *AIAA Journal*, Vol. 7, No. 2, 1969, pp. 279–285.

[7] Yurkovich, R. N., Liu, D. D., and Chen, P. C., "The State-Of-The-Art of Unsteady Aerodynamics for High Performance Aircraft," AIAA Paper 2001-0428, 2001.

[8] Romanowski, M. C., "Reduced Order Unsteady Aerodynamic and Aeroelastic Models Using Karhunen-Loeve Eigenmodes," *6th AIAA/USAF/NASA/ISSMO Symposium on Multidisciplinary Analysis and Optimization*, AIAA, Reston, VA, Sept. 1996, pp. 7–13.

[9] Kim, T., "Frequency-Domain Karhunen-Loeve Method and Its Application to Linear Dynamic Systems," *AIAA Journal*, Vol. 36, No. 11, 1998, pp. 2117–2123.

[10] Hall, K. C., Thomas, J. P., and Dowell, E. H., "Reduced-Order Modelling of Unsteady Small-Disturbance Flows Using a Frequency Domain Proper Orthogonal Decomposition Technique," AIAA Paper 99-16520, 1999.

[11] Hall, K. C., Thomas, J. P., and Dowell, E. H., "Proper Orthogonal Decomposition Technique for Transonic Unsteady Aerodynamic Flows," *AIAA Journal*, Vol. 38, No. 2, Oct. 2000, pp. 1853–1862.

[12] Willcox, K., and Peraire, J., "Balanced Model Reduction via the Proper Orthogonal Decomposition," *AIAA Journal*, Vol. 40, No. 11, Nov. 2002, pp. 2323–30.

[13] Kim, T., and Bussoletti, J. E., "An Optimal Reduced-Order Aeroelastic Modeling Based on a Response-Based Modal Analysis of Unsteady CFD Models," AIAA Paper 2001-1525, 2001.

[14] Epureanu, B. I., "A Parametric Analysis of Reduced Order Models of Viscous Flows in Turbomachinery," *Journal of Fluids and Structures*, Vol. 17, No. 7, 2003, pp. 971–982.

[15] Thomas, J. P., Dowell, E. H., and Hall, K. C., "Three-Dimensional Transonic Aeroelasticity Using Proper Orthogonal Decomposition-Based Reduced Order Models," *Journal of Aircraft*, Vol. 40, No. 3, 2003, pp. 544–551.

[16] Lieu, T., and Lesoinne, M., "Parameter Adaptation of Reduced Order Models for Three-Dimensional Flutter Analysis," AIAA Paper 2004-0888, 2004.

[17] Cizmas, P. G. A., and Palacios, A., "Proper Orthogonal Decomposition of Turbine Rotor-Stator Interaction," *Journal of Propulsion and Power*, Vol. 19, No. 2, March 2003, pp. 268–281.

[18] Spitler, J. E., "Initial Studies of Low-Order Turbulence Modeling of the Wind Turbine In-Flow Environment," AIAA Paper 2004-1004, 2004.

[19] Karhunen, K., "Zur Spektraltheorie Stochastischer Prozesse," *Ann. Acad. Sci. Fennicae*, Vol. 34, 1946.

[20] Loeve, M., "Functions aléatoire de second ordere," *Comptes Rendus de l'Academie des Sciences*, Vol. 220, 1945.

[21] Beran, P. S., and Pettit, C. L., "Prediction of Nonlinear Panel Response Using Proper Orthogonal Decomposition," AIAA Paper 2001-1292, 2001.

[22] Hong, M., Bhatia, K., SenGupta, G. T. K., Kuruvila, G., Silva, W., Bartels, R., and Biedron, R., "Simulations of a Twin-Engine Transport Flutter Model in the Transonic Dynamics Tunnel," *International Forum On Aeroelastic and Structural Dynamics*, IFAS Paper D 2003-US-44, 2003.

[23] Lieu, T., Farhat, C., and Lesoinne, M., "Reduced-Order Fluid/Structure Modeling of a Complete Aircraft Configuration," *Computer Methods in Applied Mechanics and Engineering*, Vol. 195, Nos. 41–43, 2006, pp. 5730–5742.

[24] Silva, W., and Raveh, D. E., "Development of Unsteady Aerodynamic State-Space Models from CFD-Based Pulse Responses," AIAA Paper 2001-1213, 2001.

[25] Lieu, T., "Adaptation of Reduced Order Models for Applications in Aeroelasticity," Ph.D. Thesis, University of Colorado at Boulder, Boulder, CO, 2004.

[26] Epureanu, B. I., Dowell, E., and Hall, K., "Mach Number Influence on Reduced-Order Models of Inviscid and Potential Flows in Turbomachinery," *Journal of Fluids Engineering*, Vol. 124, No. 4, 2002, pp. 977–987.

[27] Lieu, T., Farhat, C., and Lesoinne, M., "POD-Based Aeroelastic Analysis of a Complete F-16 Configuration: ROM Adaptation and Demonstration," AIAA Paper 2005-2295, 2005.

[28] Lieu, T., and Farhat, C., "Adaptation of POD-Based Aeroelastic ROMs for Varying Mach Number and Angle of Attack: Application to a Complete F-16 Configuration," AIAA Paper 2005-7666, 2005.

[29] Farhat, C., Lesoinne, M., and Maman, N., "Mixed Explicit/Implicit Time Integration of Coupled Aeroelastic Problems: Three-Field Formulation, Geometric Conservation and Distributed Solution," *International Journal for Numerical Methods in Fluids*, Vol. 21, No. 10, 1995, pp. 807–835.

[30] Lesoinne, M., Sarkis, M., Hetmaniuk, U., and Farhat, C., "A Linearized Method for the Frequency Analysis of Three-Dimensional Fluid/Structure Interaction Problems in All Flow Regimes," *Computer Methods in Applied Mechanics and Engineering*, Vol. 190, Nos. 24–25, 2001, pp. 3121–3146.

[31] Sirovich, L., "Turbulence and the Dynamics of Coherent Structures. Part 1: Coherent Structures," *Quarterly of Applied Mathematics*, Vol. 45, No. 3, Oct. 1987, pp. 561–571.

[32] Degand, C., and Farhat, C., "A Three-Dimensional Torsional Spring Analogy Method for Unstructured Dynamic Meshes," *Computers and Structures*, Vol. 80, Nos. 3–4, 2002, pp. 305–316.

[33] Farhat, C., Lesoinne, M., and LeTallec, P., "Load and Motion Transfer Algorithms for Fluid/Structure Interaction Problems with Non-Matching Discrete Interfaces: Momentum and Energy Conservation, Optimal Discretization and Application to Aeroelasticity," *Computer Methods in Applied Mechanics and Engineering*, Vol. 157, Nos. 1–2, 1998, pp. 95–114.

[34] Lesoinne, M., and Farhat, C., "CFD-Based Aeroelastic Eigensolver for the Subsonic, Transonic, and Supersonic Regimes," *Journal of Aircraft*, Vol. 38, No. 4, 2001, pp. 628–635.

[35] Holmes, P., Lumley, J. L., and Berkooz, G., *Turbulence, Coherent Structures, Dynamical Systems and Symmetry*, Cambridge Univ. Press, Cambridge, U.K., 1996.

[36] Lumley, J. L., "The Structure of Inhomogeneous Turbulence," *Atmospheric Turbulence and Wave Propagations*, edited by A. Yaglom

and V. Tatarski, Nauka, Moscow, 1967, pp. 166–178.
[37] Beran, P., "Reduced-Order Modeling: New Approaches for Computational Physics," AIAA Paper 2001-0853, 2001.
[38] Bui-Thanh, T., and Willcox, K., "Model Reduction for Large-Scale CFD Applications Using the Balanced Proper Orthogonal Decomposition," AIAA Paper 2005-4617, 2005.
[39] Taylor, J., "Dynamics of Large Scale Structures in Turbulent Shear Layers," Ph.D. Thesis, Clarkson University, Potsdam, NY, 2001.
[40] Taylor, J., and Glauser, M., "Towards Practical Flow Sensing and Control via POD and LSE Based Low-Dimensional Tools," *2002 ASME Fluids Engineering Division Summer Meeting*, ASME, Fairfield, NJ, 2002, pp. 1–9.
[41] Schmidt, R., and Glauser, M., "Improvements in Low Dimensional Tools for Flow-Structure Interaction Problems: Using Global Pod," AIAA Paper 2004-0889, 2004.
[42] Björck, Å., and Golub, G. H., "Numerical Methods for Computing Angles Between Linear Subspaces," *Mathematics of Computation*, Vol. 27, No. 123, 1973, pp. 579–594.
[43] Kunisch, K., and Volkwein, S., "Galerkin Proper Orthogonal Decomposition Methods for a General Equation in Fluid Dynamics," *SIAM Journal on Numerical Analysis*, Vol. 40, No. 2, 2002, pp. 492–515.
[44] Rathinam, M., and Petzold, L., "A New Look at Proper Orthogonal Decomposition," *SIAM Journal on Numerical Analysis*, Vol. 41, No. 5, 2003, pp. 1893–1925.
[45] Peterson, L., and Crawley, E., "Improved Exponential Time Series Approximation of Unsteady Aerodynamic Operators," *Journal of Aircraft*, Vol. 25, No. 2, 1988, pp. 121–127.

N. Alexandrov
Associate Editor